AFRL-OSR-VA-TR-2015-0099

MULTI-FUNCTIONAL UV-VISIBLE-IR NANOSENSORS DEVICES AND STRUCTURES

Michael Stroscio
UNIVERSITY OF ILLINOIS

04/29/2015
Final Report

Air Force Research Laboratory
AF Office Of Scientific Research (AFOSR)/ RTD
Arlington, Virginia 22203
Air Force Materiel Command

REPORT DOCUMENTATION PAGE

Form Approved
OMB No. 0704-0188

PLEASE DO NOT RETURN YOUR FORM TO THE ABOVE ORGANIZATION.

1. REPORT DATE *(DD-MM-YYYY)*	2. REPORT TYPE	3. DATES COVERED *(From - To)*
26-04-2015	Final	1Sep11-28Feb15

4. TITLE AND SUBTITLE
MULTI-FUNCTIONAL UV-VISIBLE-IR NANOSENSORS DEVICES AND STRUCTURES

5a. CONTRACT NUMBER

5b. GRANT NUMBER
FA9550-11-1-0271

5c. PROGRAM ELEMENT NUMBER

6. AUTHOR(S)
Michael A. Stroscio and Mitra Dutta

5d. PROJECT NUMBER

5e. TASK NUMBER

5f. WORK UNIT NUMBER

7. PERFORMING ORGANIZATION NAME(S) AND ADDRESS(ES)
Electrical and Computer Engineering Department, University of Illinois at Chicago, MC-154, 851 S. Morgan Street, Chicago, IL 60607

8. PERFORMING ORGANIZATION REPORT NUMBER

9. SPONSORING/MONITORING AGENCY NAME(S) AND ADDRESS(ES)
Air Force Office of Scientific Research
875 North Randolph Street, Suite 326, Rm 3112
Arlington, VA 22203-1768

10. SPONSOR/MONITOR'S ACRONYM(S)
AFOSR

11. SPONSOR/MONITOR'S REPORT NUMBER(S)

12. DISTRIBUTION/AVAILABILITY STATEMENT
Approved for Public Release

13. SUPPLEMENTARY NOTES

14. ABSTRACT

This research focuses on efforts underlying the enhancement of the performance of nanostructure-based sensors and electronic-optoelectronic devices. These include: initial designs of novel single-well--double-well photodetectors that significantly enhance the signal-to-noise ratio of photodetectors relying on phonon-assisted transitions as well as photon absorption events; the use of colloidal quantum dots as optoelectronic elements; investigating novel nanostructures (including graphene and CNTs as contacts) as components of quantum-dot based optoelectronic devices; investigating confined phonon effects in novel components of the integrated nanostructure-based optoelectronic structures; investigating full-tensor piezoelectric properties of nanostructures including nanowires; and the investigation of photodetector structures from these nanostructures and conducting polymers.

15. SUBJECT TERMS
nanostructures, phonon effects, piezoelectric interactions in nanostructures, conductive polymers, enhanced signal-to-noise

16. SECURITY CLASSIFICATION OF:			17. LIMITATION OF ABSTRACT	18. NUMBER OF PAGES	19a. NAME OF RESPONSIBLE PERSON
a. REPORT	b. ABSTRACT	c. THIS PAGE			Michael A. Stroscio
U	U	U	None	46	19b. TELEPHONE NUMBER *(Include area code)* 312 413 5968

Reset

INSTRUCTIONS FOR COMPLETING SF 298

1. REPORT DATE. Full publication date, including day, month, if available. Must cite at least the year and be Year 2000 compliant, e.g. 30-06-1998; xx-06-1998; xx-xx-1998.

2. REPORT TYPE. State the type of report, such as final, technical, interim, memorandum, master's thesis, progress, quarterly, research, special, group study, etc.

3. DATES COVERED. Indicate the time during which the work was performed and the report was written, e.g., Jun 1997 - Jun 1998; 1-10 Jun 1996; May - Nov 1998; Nov 1998.

4. TITLE. Enter title and subtitle with volume number and part number, if applicable. On classified documents, enter the title classification in parentheses.

5a. CONTRACT NUMBER. Enter all contract numbers as they appear in the report, e.g. F33615-86-C-5169.

5b. GRANT NUMBER. Enter all grant numbers as they appear in the report, e.g. AFOSR-82-1234.

5c. PROGRAM ELEMENT NUMBER. Enter all program element numbers as they appear in the report, e.g. 61101A.

5d. PROJECT NUMBER. Enter all project numbers as they appear in the report, e.g. 1F665702D1257; ILIR.

5e. TASK NUMBER. Enter all task numbers as they appear in the report, e.g. 05; RF0330201; T4112.

5f. WORK UNIT NUMBER. Enter all work unit numbers as they appear in the report, e.g. 001; AFAPL30480105.

6. AUTHOR(S). Enter name(s) of person(s) responsible for writing the report, performing the research, or credited with the content of the report. The form of entry is the last name, first name, middle initial, and additional qualifiers separated by commas, e.g. Smith, Richard, J, Jr.

7. PERFORMING ORGANIZATION NAME(S) AND ADDRESS(ES). Self-explanatory.

8. PERFORMING ORGANIZATION REPORT NUMBER. Enter all unique alphanumeric report numbers assigned by the performing organization, e.g. BRL-1234; AFWL-TR-85-4017-Vol-21-PT-2.

9. SPONSORING/MONITORING AGENCY NAME(S) AND ADDRESS(ES). Enter the name and address of the organization(s) financially responsible for and monitoring the work.

10. SPONSOR/MONITOR'S ACRONYM(S). Enter, if available, e.g. BRL, ARDEC, NADC.

11. SPONSOR/MONITOR'S REPORT NUMBER(S). Enter report number as assigned by the sponsoring/ monitoring agency, if available, e.g. BRL-TR-829; -215.

12. DISTRIBUTION/AVAILABILITY STATEMENT. Use agency-mandated availability statements to indicate the public availability or distribution limitations of the report. If additional limitations/ restrictions or special markings are indicated, follow agency authorization procedures, e.g. RD/FRD, PROPIN, ITAR, etc. Include copyright information.

13. SUPPLEMENTARY NOTES. Enter information not included elsewhere such as: prepared in cooperation with; translation of; report supersedes; old edition number, etc.

14. ABSTRACT. A brief (approximately 200 words) factual summary of the most significant information.

15. SUBJECT TERMS. Key words or phrases identifying major concepts in the report.

16. SECURITY CLASSIFICATION. Enter security classification in accordance with security classification regulations, e.g. U, C, S, etc. If this form contains classified information, stamp classification level on the top and bottom of this page.

17. LIMITATION OF ABSTRACT. This block must be completed to assign a distribution limitation to the abstract. Enter UU (Unclassified Unlimited) or SAR (Same as Report). An entry in this block is necessary if the abstract is to be limited.

Final Performance Report on

"MULTI-FUNCTIONAL UV-VISIBLE-IR NANOSENSORS DEVICES AND STRUCTURES,"

under Grant FA9550-11-1-0271,

1SEPTEMBER 2011 to 28 FEBRUARY 2015

Submitted to Dr. KENNETH GORETTA

April 2015

Co-PIs: Michael A. Stroscio and Mitra Dutta

Introduction: The investigators have undertaken several efforts underlying the enhancement of the performance of nanostructure-based sensors and electronic-optoelectronic devices. These include: initial designs of novel single-well--double-well photodetectors that significantly enhance the signal-to-noise ratio of photodetectors relying on phonon-assisted transitions as well as photon absorption events; the use of colloidal quantum dots as optoelectronic elements; investigating novel nanostructures (including graphene and CNTs as contacts) as components of quantum-dot based optoelectronic devices; investigating confined phonon effects in novel components of the integrated nanostructure-based optoelectronic structures; investigating full-tensor piezoelectric properties of nanostructures including nanowires; and the investigation of photodetector structures from these nanostructures and conducting polymers. This research includes modeling and theory of quantum wires and quantum dots for opto-electronic, piezoelectric, and electronic applications including sensors and piezoelectric components.

This research program addresses systematic theoretical and experimental investigations of nanostructure-based electronic and optoelectronic structures with the goal of facilitating major improvements in the performance levels of nanodevices beyond the current state-of-the-art. In particular, this program focuses on research thrusts with objectives including: model, design, fabricate, and experimentally characterize robust multi-functional nano-device structures for enhanced charge transport & collection; model, design, fabricate, and experimentally characterize such nanodevices to optimize device structures with quantum-engineering and phonon-assisted transitions in nanostructures. Quantum engineering of nano-structures is emphasized. Related quantum-wire structures – including piezoelectric quantum wires are included.

Important results obtained during effort include: electrical and optical studies of components of devices and systems of quantum-dot-based optoelectronic devices; electronic and optical properties of quantum dots and quantum wires; characterization of phonon modes and piezoelectric interaction in quantum wires; and extending a theory band formation in an array of colloidal quantum dots embedded in conductive polymer; extending a theory band formation in an array of colloidal quantum dots embedded in conductive polymer; initial design of a novel single-well double-well heterostructure photodetectors with dramatically enhance signal-to-noise based on resonant interface-phonon-assisted transitions; role of interface optical phonon modes in wurtzite quantum heterostructures; and interface phonon modes of dual-gate MOSFETs.

Specific results were obtained on the following topics:

Design of a Novel Heterostructure Photodetectors with Dramatically Enhance Signal-to-Noise based on Resonant Interface-Phonon-Assisted Transitions and Engineering of Energy States to Enhance Transition Rates;

Effect of the Size and the Separation of Metal Nanodots on the Electromagnetic Enhancement to Surface-enhanced Raman Spectroscopy;

Interface Optical Phonon Modes in Wurtzite Quantum Heterostructures;

Interface Phonon Modes of Dual-Gate MOSFET Systems;

Phonon bottleneck effects in rectangular graphene quantum dots;

Theoretical study on the effect of piezoelectric charges on the surface potential and surface depletion region of ZnO nanowires;

Modeling the effect of nanowire size on the piezoelectric effects;

Interface phonon modes in wurtzite heterostructure systems;

Effect of the size and the separation of metal nanodots on the electromagnetic enhancement to surface-enhanced Raman spectroscopy;

Annealing-induced morphological changes in nanocrystalline quantum dots and their impact on charge transport properties;

Photoluminescence and Raman Spectroscopy of Polycrystalline ZnO Nanofibers Deposited by Electrospinning;

Piezoelectricity in Wurtzite Polar Semiconductor Nanowires: A Theoretical Study;

Electronic Properties of Y-junctions in SnO_2 Nanowires;

Tailoring the Surface Properties and Carrier Dynamics in SnO_2 Nanowires;

Charge Transport in Two Conductive Polymer and Semiconducting Quantum Dot Nanocomposite Systems;

Piezoelectricity in Zinc Blende Polar Semiconductor Nanowires: A Theoretical Study;

Piezoelectricity in Lead Zirconate Titanate Semiconductor Nanowires: A Theoretical Study;

Electronic properties in surface passivated SnO_2 nanowires with Schottky contacts;

Phonon bottleneck effects in rectangular graphene quantum dots;

Piezoelectric Fields in Quantum Wires;

Optoelectronic Applications of Colloidal Quantum Dots.

In this Final Report summaries are organized in the follow Sections:

Section I: Initial Design of Photodetectors using Quantum Engineering of Electronic States and Phonon Engineering

Enhanced Signal-to-Noise in Photodetectors due to Interface Phonon-assisted Transitions

Yi Lan, Nanzhu Zhang, Junxia (Lucy) Shi, M. Dutta and M. A. Stroscio
Department of Electrical and Computer Engineering
University of Illinois at Chicago
Chicago 60607, United States
ylan3@uic.edu

***Abstract*—Herein, we consider examine the possibility of photodetectors with reduced signal-to-noise based on a three quantum well structure with one single well and one double well. This structure facilitates photon detection through the following sequence of events: photon absorption, phonon emission, and then photon absorb of a photon having the same wavelength as the first one. Even though this design two photons a phonon-assisted transition, it is demonstrated that greatly enhance signal-to-noise is obtained.**

Keywords—single-double quantum wells; photon; phonon; photodetector)

I. INTRODUCTION

This paper addresses novel photodetectors with dramatic enhancement in detectivity, based on rapid interface phonon-assisted transitions combined with quantum engineering of phonon and electron states in nanostructures. Based on the concepts we introduced previously [1-2] for heterosturcture lasers, which have resulted in extremely large enhancements in the optical gain of quantum-well-based lasers, this work examines dramatic enhancement of photodetectivity in novel quantum-well based photodetectors in the first known embodiment that facilitates the detection of photons over a wide range of frequencies. Herein, we consider a triple quantum-well structure with one single well and one double well; the relationship between the energy levels should be, as in Fig. 1.

$E_3 = E_2$'
$E_3 - E_1 = E_4' - E_2 = E_{photon}$
$E_2' - E_2 = E_{phonon}$

This energy-level structure facilitates the absorption of a photon, emission of a phonon, and the absorption of a photon with the same wavelength as the original photon. E_1 is the first energy level of the single well, and E_3 is the second energy level of it. In addition, E_2, E_2', E_4, and E_4' represent the first, second, third, and forth energy levels for the double quantum well.

With reference to Fig. 1, it is straightforward to see that there will be a dramatic signal-to-noise enhancement in the current, $I_{sn,E1}$, from the deepest state E_1, relative to $I_{sn,E2}$, from the deepest state E_2 (without phonon-assisted transition and second photon absorption), as given by the Richardson formula:

$$\frac{I_{sn,E_1}}{I_{sn,E_2}} = \frac{e^{-\frac{2E_{photon}-E_{phonon}}{kT}}}{e^{-\frac{E_{photon}}{kT}}} = e^{-\frac{E_{photon}-E_{phonon}}{kT}} \quad (1)$$

In this equation, $E_3 - E_1 = E_4' - E_2 = E_{photon}$ and $E_2' - E_2 = E_{phonon}$.

For example if $\frac{E_{photon}-E_{phonon}}{kT} = 8$, a dramatic 1/3,000 reduction can be realized.

II. THEORETICAL MODEL

A. Single-Double quantum well Structure

Design a three quantum wells structure with one single well and one double well as Figure 1.

The relationship between the energy levels should be E_3 equals to E_2', and the difference between E_3 and E_2, which is also the first splitting of the double quantum well, equals to one phonon energy. The difference between E_3 and E_1, and the difference between E_4' and E_2 should be the same and equal to one photon energy.

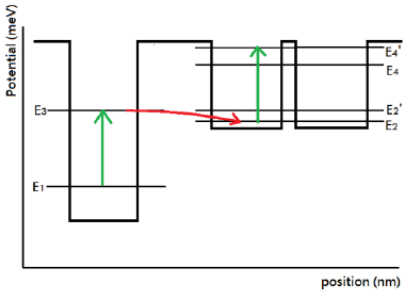

Figure 1. Structure of photodetector.

Therefore, we can have it absorbing a photon, emitting a phonon, and then absorbing a same wavelength of photon. E_1 is the first energy level of the single well, and E_3 is the second energy level of it. At the meanwhile, E_2, E_2', E_4, and E_4' represent the first, second, third, and forth energy level for the double quantum well.

978-1-4799-5433-9/14/$31.00 ©2014 IEEE

Proceedings of the International Workshop on Computational Electronics, IEEE

B. *Transfer Efficiency*

Considering the transfer efficiency, from the Fermi's Golden Rule [1],

$$\frac{1}{\tau_i} = \frac{2\pi}{\hbar}\sum_f \left|\langle f|\tilde{H}|i\rangle\right|^2 \delta(E_f - E_i) \qquad (2)$$

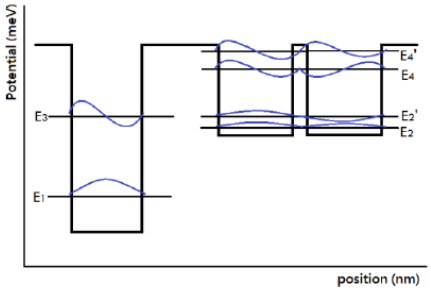

Fig. 2 Wavefunctons of photodetector.

To have large transfer efficiency, we would like the multiplication of wave functions at initial and final state, and the phonon/photon energy to be even. Therefore, we could have them (even odd odd) or (even even even). As we know, photon energy is odd, and phonon energy is asymmetric (odd) as well. We need one energy level having wave function to be even, and another one to be odd.

From figure 2. it shows that E_1 E_2 E_4 are even, but E_3 E_2' E_4' are odd.

We pick E_1 to E_3, and E_2 to E_4' as the photon absorbing levels; the splitting of E_2' to E_2 as phonon emitting levels.

C. *Energy Levels*

For calculating the energy levels in the quantum wells, we use the Schrödinger equation with effective mass mismatch at heterojunctions [2].

$$\begin{aligned} -\frac{\hbar^2}{2m_b^*}\frac{\partial^2}{\partial z^2}\psi(z) + V\psi(z) &= E\psi(z), \quad && z \le -\frac{l_w}{2} \\ -\frac{\hbar^2}{2m_w^*}\frac{\partial^2}{\partial z^2}\psi(z) &= E\psi(z), \quad && -\frac{l_w}{2} \le z \le \frac{l_w}{2} \\ -\frac{\hbar^2}{2m_b^*}\frac{\partial^2}{\partial z^2}\psi(z) + V\psi(z) &= E\psi(z), \quad && \frac{l_w}{2} \le z \end{aligned} \qquad (3)$$

Then we need to compute the interface phonon modes of our structure cause we need to make sure E_2'-E_2=E_{phonon} in our structure.

III. Model Examples

Detector designs have been considered using several different materials, and herein designs based on GaAlAs, InGaAs, and InAlAs/InP are considered.

A. *GaAlAs Design*

For GaAs/$Ga_{1-x}Al_xAs$, band Gap, Eg= (1.426+1.247x) eV; band alignment: 33% of total discontinuity in valence band, i.e. ΔV_{VB}=0.33; ΔV_{CB}=0.67; and electron effective mass, m*= (0.067+0.083x) m_0 [1].

According to the GaAlAs design as figure 3. we got the first photon absorbing by the single having the energy of 211.193 meV, and the second photon absorbing by the double well having the energy of 206.23 meV. And the error is 2.407%.

We want E_3 equals to E_2' as well. The difference here is 0.23 meV.

The phonon energy in Figure 3 is 33.79 meV, but after calculating the interface phonon in this structure, we can find one phonon at 33.812 meV. The error is only 0.067%, which is very small.

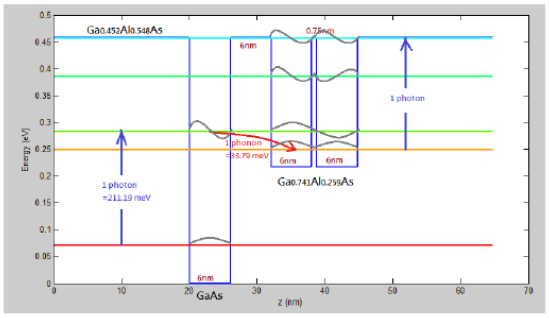

Figure 3. GaAlAs structure with E_1=0.07117 meV, E_3=0.28231 meV, E_2=0.24852 meV, E_2'=0.28225 meV, E_4=0.38471 meV, E_4'=0.45475 meV. Potential for the single quantum well is 457.849meV, and for double well is 241.457 meV.

B. *InGaAs Design*

For $In_{1-x-y}Al_xGa_yAs$/AlAs, total band discontinuity, $\Delta V = [2.093x + 0.629y + 0.577x^2 + 0.436y^2 + 1.013xy - 2.0x^2(1-x-y)]$ eV

Band alignment: 47% of total discontinuity in valence band, i.e. ΔV_{VB}=0.47; ΔV_{CB}=0.53; and electron effective mass, m*= (0.0427+0.0685x) m_0 [1]. Therefore, for $In_{1-y}Ga_yAs$/AlAs, $\Delta V = [(0.629y + 0.436y^2) \times 0.53]$ eV in conduction band. Effective mass=, m*= (0.0427) m_0.

According to the InGaAs design as Figure 4, we got photon absorption by the single well having the energy of 170.566 meV, and the second photon absorbed by the double well having the energy of 177.4 meV. In experiment, error less than 5% is acceptable. And the error in this case is 4%.

The difference between E_3 and E_2' is 0.23 meV.

The phonon energy in this case is 33.9 meV, but after calculating the interface phonon in this structure, we can find one phonon at 33.619 meV. The error is only 0.83%.

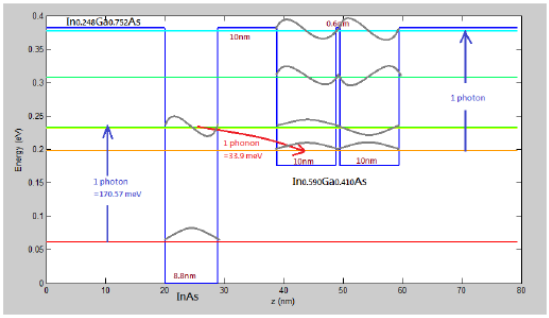

Figure 4. InGaAs structure with E_1=0.061614 meV, E_3=0.23218 meV, E_2=0.19828 meV, E_2'=0.23195 meV, E_4=0.30754 meV, and E_4'=0.37568 meV. Potential for the single quantum well is 381.371 meV, and for double well is 205.845 meV.

C. InAlAs/InP Design

From the parameters of $In_{1-x-y}Al_xGa_yAs/AlAs$ we mentioned at part *B*, for $In_{1-x}Al_xAs/AlAs$, $\Delta V = [(2.093x - 1.423x^2 + 2x^3) \times 0.53]$ eV in the conduction band. Effective mass=, m*= (0.0427+0.0685x) m_0.

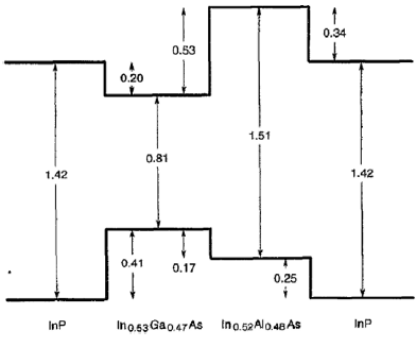

Figure 5. Calculated valence-band offsets are combined with measured low-temperature band gaps to yield the energy band diagram (in eV) for the heterointerface in the InGaAs/InAlAs/InP family [3].

The information from Figure 5 is used to calculate the relationship of energy levels between InAlAs and InP.

For the InAlAs/InP design as Figure 6, the first photon is absorbed in the single well having the energy of 239.525 meV, and the second photon is absorbed in the double well having the energy of 236.81 meV. And the error is 1.136%.

The difference between E_3 and E_2' is 2.17 meV.

The phonon energy in this case is 30.2 meV, but after calculating the interface phonon in this structure, we can find one phonon at 29.19 meV. The error is only 3.46%.

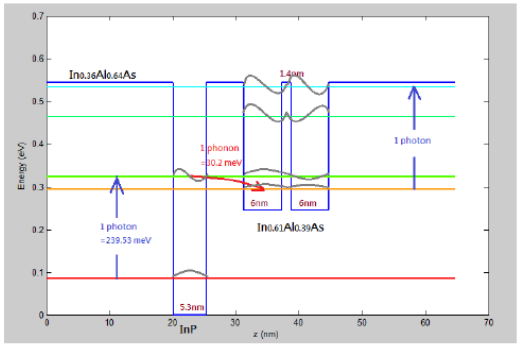

Figure 6. InAlAs/InP structure with E_1=0.085365 meV, E_3=0.32489 meV, E_2=0.0.29469 meV, E_2'=0.32272 meV, E_4=0.4623 meV, E_4'=0.5315 meV. Potential for the single quantum well is 542.981meV, and for double well is 298.113 meV.

IV. Phonon Energy Calculation

The interface phonon modes of our structure produce a rapid phonon-assisted transfer of electrons [4, 5, 6] when E_2'-E_2=E_{phonon} in our structure.

For the photodetector modeled here, there are five interfaces. In order to calculate the potential in our system, we then write the potentials of the seven regions as the following:

$$\begin{cases} \Phi = Ae^{qz} & z < 0 \\ \Phi = Be^{qz} + Ce^{-qz} & 0 \le z \le d_1 \\ \Phi = De^{q(z-d_1)} + Ee^{-q(z-d_1)} & d_1 \le z \le d_2 \\ \Phi = Fe^{q(z-d_2)} + Ge^{-q(z-d_2)} & d_2 \le z \le d_3 \\ \Phi = He^{q(z-d_3)} + Ie^{-q(z-d_3)} & d_3 \le z \le d_4 \\ \Phi = Je^{q(z-d_4)} + Ke^{-q(z-d_4)} & d_4 \le z \le d_5 \\ \Phi = e^{-q(z-d_5)} & z > d_5 \end{cases} \quad (4)$$

Where A, B, C, D, E, F, G, H, I, J and K are constants. At the heterointerfaces of the six regions, the following two conditions have to be satisfied [5]:

$$\Phi_1(Z) = \Phi_2(Z) \quad (5)$$

$$\varepsilon_1 \frac{\partial \varepsilon_1}{\partial z} = \varepsilon_2 \frac{\partial \varepsilon_2}{\partial z} \quad (6)$$

Then we can get the secular equation of our system,

$$\frac{Je^{q(d_5-d_4)} + Ke^{-q(d_5-d_4)}}{Je^{q(d_5-d_4)} - Ke^{-q(d_5-d_4)}} = -\frac{\varepsilon_3}{\varepsilon_1} \quad (7)$$

Where ε_1 is the dielectric function of the substrate, ε_3 is the dielectric function of the double quantum well.

Solving this equation yields the interface phonon modes of our system.

As long as we have the interface phonon modes, we can then calculate the potential by using the following normalization condition:

$$\frac{\hbar}{2\omega L^2} = \sum \frac{1}{4\pi}\frac{1}{2\omega}\frac{\partial \varepsilon_i(\omega)}{\partial \omega}\int_{\tilde{S}_i} dz(q^2|\Phi_i(q,z)|^2 + \left|\frac{\partial \Phi_i(q,z)}{\partial z}\right|^2) \quad (8)$$

Substituting the potentials into this condition, it becomes:

Here we substitute the relationship between these constants we obtained from the previous boundary conditions into this condition we can get an equation

Which has just one unknown A. The Frohlich potential for

$$\begin{aligned}
&\frac{\partial \varepsilon_1(\omega)}{\partial \omega} qA^2 + \frac{\partial \varepsilon_2(\omega)}{\partial \omega} q(B^2(e^{2q\delta_1} - 1) + C^2(1 - e^{-2q\delta}))) + \\
&\frac{\partial \varepsilon_3(\omega)}{\partial \omega} q(D^2(e^{2q(d_3 - d_1)} - 1) + E^2(1 - e^{-2q(d_3 - d_1)})) \\
&+ \frac{\partial \varepsilon_3(\omega)}{\partial \omega} q(F^2(e^{2q(d_3 - d_2)} - 1) + G^2(1 - e^{-2q(d_3 - d_2)})) \\
&+ \frac{\partial \varepsilon_3(\omega)}{\partial \omega} q(H^2(e^{2q(d_4 - d_2)} - 1) + I^2(1 - e^{-2q(d_4 - d_2)})) \quad (9) \\
&+ \frac{\partial \varepsilon_3(\omega)}{\partial \omega} q(J^2(e^{2q(d_3 - d_4)} - 1) + K^2(1 - e^{-2q(d_3 - d_4)})) - \frac{\partial \varepsilon_1(\omega)}{\partial \omega} q = \frac{4\pi\hbar}{L^2}
\end{aligned}$$

the phonon-assisted transitions follows straightforwardly. These families interface LO phonons have facilitate achieving rapid (ca. 0.1 ps as in Ref [6]) resonant phonon-assisted transitions between the single-well and double-well regions of Figures 1-6.

V. Discussion

In conclusion, we have employed quantum engineering of electronic states and phonon dispersion conditions to engineer single-well—double-well photodetector heterostructures that have signal-to-noise ratios enhanced by several orders of magnitude by using phonon-assisted transitions. Using this model, we have identified several different structures – with specific materials, compositions -- suitable as photodetectors incorporating phonon-assisted transitions: one based on GaAlAs/GaAs material system, one based on InGaAs/InAs material system and the other one base on InAlAs/InP material system. These designs bear similarities to phonon-assisted quantum cascade lasers [7-9].

Work supported, in part, under AFOSR Grant FA9550-11-1-0271.

References

[1] Paul Harrison, Quantum Wells, Wires and Dot: Theoretical and Computational Physics, 3rd edition, (Wiley, New York, 2010).

[2] A. R. Bhatt, K. W. Kim, M. A. Stroscio, G. J. Iafrate, Mitra Dutta et al, *Reduction of interface phonon modes using metalsemiconductor heterosturctures*, Journal of Applied Physics 73, 2338 (1993).

[3] Hybertsen, Mark S.K., Band offset transitivity at the InGaAs/InAlAs/InP(001) heterointerfaces, Applied Physics Letters, Volume 58, Issue 16, April 22, 1991, pp.1759-1761.

[4] Michael A. Stroscio, Interface-Phonon--Assisted Transitions in Quantum Well Lasers, Journal of Applied Physics, 80, 6864 (1996); see also M. Stroscio and M. Dutta, Phonons in Nanostructures (Cambridge University Press. 2001).

[5] Mikhail V. Kisin, Vera B. Gorfinkel, Michael A. Stroscio, Gregory Belenky, and Serge Luryi, Influence of Complex Phonon Spectra on Intersubband Optical Gain, Journal of Applied Physics, 82, 2031 (1997).

[6] Michael A. Stroscio, Mihail Kisin, Gregory Belenke, and Serge Luryi, Phonon enhanced inverse population in asymmetric double quantum wells, Appl. Phys. Letts., 75, 3258-3260 (1999).

[7] V. Spagnolo, G. Scamarcio, M. Troccoli, F, Capasso, C. Gmachl, A. M. Sergent, A. L. Hutcheson, D. L. Sivco, and A. Y. Cho, Nonequilibrium Optical Phonon Gen. by Steady State Electron Transport in Quantum-Cascade Lasers, APL, 80, 4303-4305 (2002)

[8] 5. B. S. Williams, B. Xu, Q. Hu, Narrow-linewidth Terahertz Emission from Three-level Systems, APL, 75, 2927 (1999)

[9] 6. V. M. Menon, L. R. Ram-Mohan, W. D. Goodhue, A. J. Gatesman, A. S. Karakashian, Role of Interface Phonons in Quantum Cascade Terahertz Emitters, Physica B, 316-317, 212-215 (2002).

Section II: Growth of Nanowires: Photoluminescence Properties and Harmonic Generation of Phonons

Journal of ELECTRONIC MATERIALS, Vol. 43, No. 11, 2014
DOI: 10.1007/s11664-014-3305-0

Characterization of CdS Nanowires Self-Assembled in a Nanoporous Alumina Template

SHRIPRIYA PODURI,[1] MITRA DUTTA,[1,2,4] and MICHAEL STROSCIO[1,2,3]

1.—Department of Electrical and Computer Engineering, University of Illinois at Chicago, Chicago, IL 60607, USA. 2.—Department of Physics, University of Illinois at Chicago, Chicago, IL 60607, USA. 3.—Department of Bioengineering, University of Illinois at Chicago, Chicago, IL 60607, USA. 4.—e-mail: dutta@uic.edu

CdS nanowires were self-assembled in a thin film (~200 nm) anodic aluminum oxide template on an indium tin oxide-coated glass substrate via dc electrodeposition. Raman spectral studies were done to probe the vibrational properties of scattering CdS phonons. Strong 1 longitudinal optical (LO), 2 LO, and 3 LO peaks were observed at 302 cm^{-1}, 603 cm^{-1}, and 906 cm^{-1} having an energy separation of 37 meV, which is in accordance with the CdS bulk values. The photoluminescence spectra showed improved intensity of emission on annealing of the CdS nanowires. Field-emission scanning microscopy confirms the growth of nanowires of diameters ranging from 10 nm to 25 nm for these templates. These diameters agreed with those extracted from the luminescence emission energies.

Key words: CdS nanowire, longitudinal optical, anodic aluminum oxide

INTRODUCTION

Semiconductor nanoscale structures have generated a great deal of interest owing to their strong confining potentials for electrons and holes and the associated quantum effects. Semiconductor nanowire devices are being widely used as sensors, light-emitting diodes (LEDs), photon emitters, and lasers.[1–7] In order to grow free-standing nanowire arrays and to achieve standing nanowire arrays, large periodic arrays of nanoporous structures need to be fabricated. Anodic aluminum oxide (AAO) templates are used for growing nanowires by electrochemical deposition since this nanoporous structure is uniform and has an almost regular array of nanopores. The diameters of the nanopores can be easily varied by changing the experimental parameters of anodization. One of the prototypical II-IV semiconductor compounds, cadmium sulfide (CdS), was selected because of the possible use in optical devices due to its direct band gap in the visible spectral range and the excellent semiconducting properties. Although there are different methods reported for the synthesis of CdS nanowires, such as chemical vapor deposition and vapor–liquid–solid growth,[8,9] template-based synthesis of nanowires via dc or ac electrodeposition is attractive due to its low cost, and easy fabrication process.

CdS nanowires were self-assembled in an anodic aluminum template of 200 nm thickness on indium tin oxide (ITO)-coated glass. In this paper, Raman and photoluminescence spectral studies were performed to probe the vibrational and electronic states of the CdS nanowires grown via dc electrodeposition. The topographical features of these CdS nanowires were also studied using field emission scanning electron microscopy.

(Received November 22, 2013; accepted June 27, 2014; published online July 29, 2014)

EXPERIMENTAL DETAILS

Commercially available ITO-coated 1″ × 1″ (c. 25 mm × 25 mm) glass substrate (1 mm thick) were ultrasonicated in acetone and isopropanol to clean the substrate to remove the organic residues, followed by the deionized water rinse and air gun blow dry. A thin layer of aluminum (~200 nm thick) was deposited at a rate of 0.2 nm/s using e-beam evaporation. Prior to the deposition of aluminum, an interlayer of titanium of 5 nm thickness was

deposited between the Al and ITO. This was to prevent the poor connectivity and delamination of aluminum during anodization from the ITO-coated glass.[10,11] The interlayer of the Ti layer was deposited using e-beam evaporation and there was no vacuum break between the Ti and Al layers.[12] These templates were anodized at a potential of 30 V and current of 0.2 A to develop the nanopores in oxalic acid. The anodized template was heated in a mixture of phosphoric acid (5 wt.%) and chromic acid (10 wt.%) at 60°C to remove the aluminum oxide layer and excess of aluminum. Since the pores that appeared during the first anodization step were poor and non-uniform, the anodized template was again anodized at a potential of 40 V and 0.2 A in 0.3 M oxalic acid at 2–8°C. The nanopores produced in the template were 10–60 nm in diameter. The diameters of the pores were controlled by varying the anodization parameters such as temperature and also with the pH of the acid used according to the protocol of Ref. 13.

After the two-step anodization, very uniform pores of 10–60 nm developed, but growth was accompanied by a barrier layer of oxide at the interface of the Al and Al_2O_3. This aluminum oxide barrier layer and non-uniformity in barrier layer thickness causes some problems affecting the growth and quality of the nanowires electrodeposited in the pores, resulting in much lower filling of nanowires in these pores. The barrier layer can be removed by dipping the substrate in 5% by weight phosphoric acid (H_3PO_4) for 3–4 min. The barrier layer which is formed at the bottom of the template can be removed by either 5% by weight phosphoric acid or dry etch with chlorine-based gases,[12–14] but, as shown in the referenced work, the barrier layer can be removed with the phosphoric acid etch without damaging the template.

It has been reported that ac electrodeposition in an AAO template is the most efficient process to fabricate aligned CdS nanowires.[13–16] In this paper, however, CdS nanowires were cathodically depos-

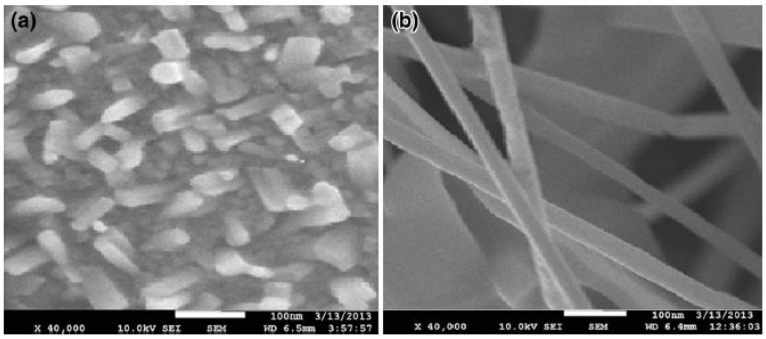

Fig. 1. (a) Top view, (b) side view SEM micrograph of CdS nanowires of 10–20 nm in diameter before annealing.

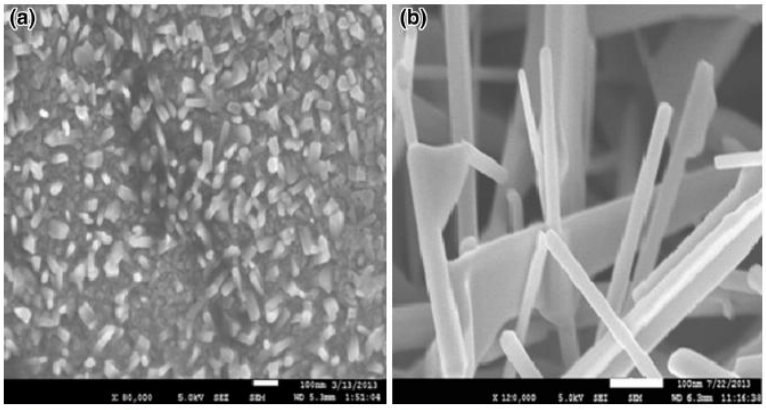

Fig. 2. (a) Top view, (b) side view SEM micrograph of CdS nanowires of 10–20 nm in diameter after annealing.

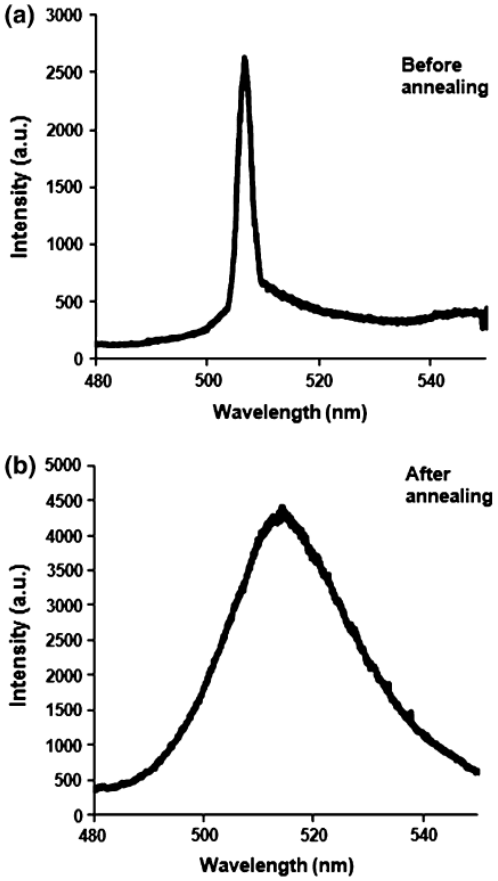

Fig. 3. (a) PL spectra of as grown CdS nanowires with peak at 506 nm. (b) PL spectra of CdS nanowires which were annealed at 500°C for 1 h with peak at 514 nm.

ited via dc electrodeposition. DC electrodeposition of CdS nanowires is not very commonly done for samples with very narrow pore diameters.[13] However, in our work, CdS nanowires were grown by using a simple dc electrodeposition process into the narrow pores of 10–60 nm diameter. While it has been stated in Ref. 13 that DC electrodeposition was not an easy process for growing nanowires in narrow pores, we were able to achieve the growth of CdS nanowires of decent quality. The electrolyte for CdS electrodeposition was composed of 0.055 M $CdCl_2$ and 0.19 M elemental sulfur, dissolved in dimethyl sulfoxide (DMSO).[17,18] The temperature of the electrolyte was maintained at 120–150°C, and a constant current density of 15 mA/cm^2 was applied for 7–10 s with the deposition rate at 25–30 nm/s. After the electrodeposition, the samples were rinsed in hot DMSO followed by acetone and deionized water rinse. The CdS nanowires were liberated by dissolving the AAO templates in 1 M NaOH solution at room temperature for 8 min after which they were completely dissolved. These nanowires were annealed at 500°C for 1 h for improving their crystallinity.

Field emission scanning electron microscopy (FESEM) imaging was performed using a JEOL 7500 FESEM to study the morphology and ascertain the growth of the nanowires. Raman scattering and photoluminescence spectral studies were employed to investigate the longitudinal optical phonon modes and the electronic states of the CdS nanowires.

RESULTS AND DISCUSSION

Fabricating CdS nanowires using an AAO template is a complicated procedure due to the presence of a barrier layer of aluminum oxide which is difficult to remove completely, thus causing nonuniformities in the growth of the nanowires, and also the template must be free of cracks and defects.[19,20] The electrodeposition of CdS nanowires comprises three steps.

Firstly, the elemental sulfur in the solution dissociates into S^{2-} ions. Secondly, the $CdCl_2$ also dissociates into Cd^{2+} ions. Thirdly, these S^{2-} ions react with the Cd^{2+} ions in the solution to form CdS crystallites inside the nanopores of the template, thus forming the nanowires.[21] These crystallites nucleate on the walls of pores initially forming nanotubes, and gradually these nanotubes get filled up with CdS crystallites forming nanowires.[22]

The surface morphology of these CdS nanowires grown in the AAO template were investigated using the JEOL FESEM after the dissolution of the AAO template in 1 M NaOH solution for 5–8 min. The SEM micrographs of CdS nanowires before and after the annealing are shown in Figs. 1 and 2, respectively, which confirms the growth of nanowires of average diameter of approximately 10–25 nm.

The photoluminescence (PL) of the as-grown CdS nanowires were investigated using a He-Cd laser of wavelength 325 nm for excitation at room temperature. The PL spectra for the as-grown CdS nanowires after dissolution of the AAO template in 1 M NaOH solution is shown in Fig. 3a where there is an emission peak at 506 nm attributed to some of the CdS nanowires. This emission is somewhat weak.

However, after annealing in nitrogen gas for 1 h at 500°C, the emission became substantially stronger and broader and the emission peak moved closer to the bulk value of 2.42 eV, and the intensity of the emission (the area under the PL peak) also increased by a factor of 4.36 as shown in Fig. 3b. The narrow peak at higher energy before the annealing is due to the confinement in the few narrow wires that are of better quality. After annealing, the total intensity is increased but the line width is broader and encompasses both narrow

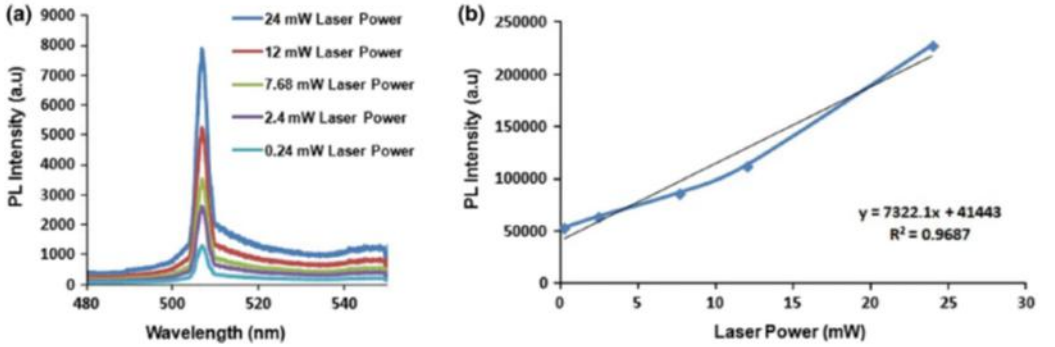

Fig. 4. (a) PL spectra of CdS nanowires with different laser excitation power using neutral density filters before annealing. (b) PL intensity area variation versus different laser excitation power using neutral density filters before annealing.

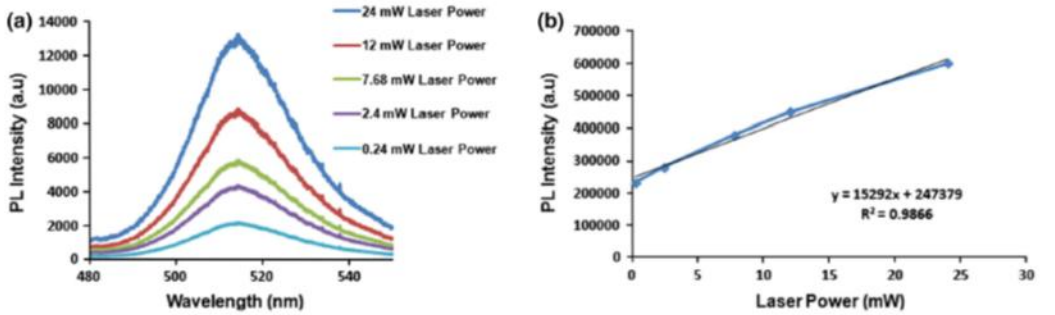

Fig. 5. (a) PL spectra of CdS nanowires with different laser excitation power using neutral density filters after annealing. (b) PL intensity area variation versus different laser excitation power using neutral density filters after annealing.

and wider wires which were likely not luminescent earlier due to defects which were annealed out. Thus, after annealing, the peak moved to a lower energy where the PL is centered at the value for wider wires. It is also possible that some of the increased signal can partially be from the bulk region where there are no wires, but mainly the luminescence must still be from nanowires since the feature is broad and the SEM pictures show distinct nanowires.

In other work, however, after annealing the sample at 500°C for 1 h in nitrogen, the shifting of the emission peak to the higher wavelength has also been observed.[21] This change in luminescence emission indicates that the array has a distribution of nanowire diameters and that there are more nanowires of different diameters becoming involved in the emission process after annealing. Also, the photoluminescence power dependence was studied for the identification of underlying recombination methods. PL was performed before and after annealing with different neutral density filters (purchased from Thorlabs) to evaluate the crystal quality.[23] The PL spectral intensity for various transmission laser power density percentages before and after annealing is shown in Fig. 4a, b, and the plot for the PL intensity with respect to various transmission laser power density percentages is in Fig. 5. The plot of PL intensity area under the curve with respect to different excitation power is a near linear plot with a positive slope which improves in linearity on annealing, thus showing that the recombination was mainly band to band. From the plots one can see that there were some defect states prior to annealing, but after the annealing the linearity with intensity improved. We thus see a slight shift of peak from 506 nm to 514 nm.

Assuming the nanowires as an infinite one-dimensional quantum well of width a, which is the diameter of the nanowire, the excitation caused by the 325-nm laser is explained by Eq. 1[24]:

$$E_g^{CdS} = E_g^{bulk} + \frac{h^2}{8m_o a^2}\left(\frac{1}{m_e} + \frac{1}{m_h}\right). \quad (1)$$

After solving the equation with E_g^{CdS} at 506 nm and 514 nm, E_g^{bulk} as 2.4 eV and also taking the

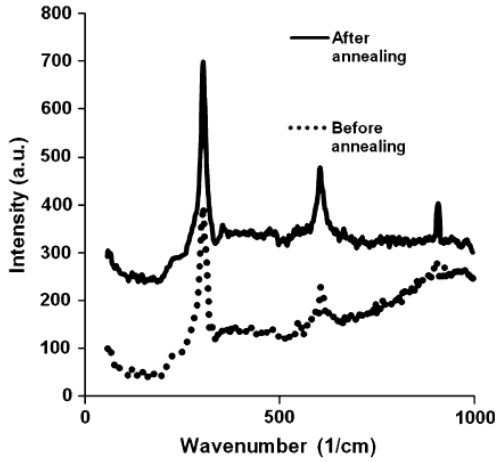

Fig. 6. Raman peaks observed at 302 cm^{-1}, 603 cm^{-1}, 906 cm^{-1} corresponding to 1LO, 2LO, and 3LO of CdS nanowires, respectively.

effective mass of CdS as reported in Ref. 25, we get the diameter of nanowires as 7.01 nm for those with a peak at 506 nm and 16 nm for those with a peak at 514 nm, respectively, which is approximately very close to the actual diameter range (10–25 nm) of the nanowires, as can be seen in Fig. 2b. The very simple model and the likely depletion layer can cause the calculated values to be somewhat smaller than the actual observed nanowire diameters.

The Raman spectrum of these annealed CdS nanowires was recorded using an Ar^+ ion laser of 514 nm wavelength. The Raman characteristics of these nanowires before and after annealing are shown in Fig. 6. Raman peaks were observed at 302 cm^{-1}, 603 cm^{-1}, and 906 cm^{-1} corresponding to the longitudinal optical phonon (LO) modes 1LO, 2LO, and 3LO, respectively, analogous to the peaks of pure CdS crystalline structure.[8,26] Strong 1LO, 2LO, and 3LO peaks were observed with stronger peaks after annealing.

CONCLUSION

To grow nanowires in na anoporous template is a complicated procedure in a nanoporous AAO thin template of 200 nm because of its susceptibility to crack and its poor connectivity to the substrate. We have employed a simple dc electrodeposition procedure to self-assemble CdS nanowires in a thin AAO template and briefly describing the fabrication issues at each fabrication step. It is a highly advantageous procedure to grow nanowires in an AAO template because of its ability to withstand high temperature, high reproducibility, and easy to fabricate large arrays of nanowires of high aspect ratios. CdS nanowires grown with this method were characterized using scanning electron microscopy, photoluminescence, and Raman spectra showing good crystallinity of CdS nanowires before and after annealing.

ACKNOWLEDGEMENTS

This work was supported in part by AFOSR Grant under FA9550-11-1-0271.The author, Shripriya Poduri was supported, in part, by Lam Research Corporation.

REFERENCES

1. J.R. Heath, P.J. Kuekes, G. Snyder, and R.S. Williams, *Science* 280, 1717 (1998).
2. G.T. Hu, T.W. Odom, and C.M. Lieber, *Acc. Chem. Res.* 32, 435 (1999).
3. A.M. Morales and C.M. Lieber, *Science* 279, 208 (1998).
4. R. Agarwal, C.J. Barrelet, and C.M. Lieber, *Nano Lett.* 5, 917 (2005).
5. X. Duan, Y. Huang, Y. Cui, J. Wang, and C.M. Lieber, *Nat. Lond.* 409, 66 (2001).
6. M.T. Borgstrom, V. Zwiller, E. Muller, and A. Imamoglu, *Nano Lett.* 5, 1439 (2005).
7. X. Duan, Y. Huang, R. Agarwal, and C.M. Lieber, *Nat. Lond.* 421, 241 (2003).
8. A. Abdi, L.V. Titova, L.M. Smith, H.E. Jackson, J.M. Yarrison-Rice, and J.L. Lauhon, *Appl. Phys. Lett.* 88, 043118 (2006).
9. S. Kar and S. Chaudhuri, *J. Phys. Chem. B* 110, 4542 (2006).
10. P. Liu, V.P. Singh, C.A. Jarro, and S. Rajaputra, *IOP Nanotechnol.* 22, 145304 (2011).
11. T.R.B. Foong, A. Sellinger, and X. Hu, *ACS Nano* 11, 2250 (2008).
12. A. Yin, M. Tzolov, D.A. Cardimona, and J. Xu, *IEEE Trans. Nanotechnol.* 5, 564 (2006).
13. D. Routkevitch, T. Bigioni, M. Moskovits, and J.M. Xu, *J. Phys. Chem.* 100, 14037 (1996).
14. P. Liu, V.P. Singh, and S. Rajaputra, *IOP Nanotechnol.* 21, 115303 (2010).
15. D. Routkevitch, T.L. Haslett, L. Ryan, T. Bigioni, C. Douketis, and M. Moskovits, *Chem. Phys.* 210, 343 (1996).
16. J.L. Hutchison, D. Routkevitch, M. Moskovits, and R.R. Nayak, *Inst. Phys. Conf. Ser.* 157, 389 (1997).
17. D. Xu, Y. Xu, D. Chen, G. Guo, L. Gui, and Y. Tang, *Chem. Phys. Lett.* 325, 340 (2000).
18. Y. Yang, H. Chen, Y. Mei, J. Chen, X. Wu, and X. Bao, *Solid State Commun.* 123, 279 (2002).
19. J.D. Klein, R.D. Herrick, D. Palmer, M.J. Sailor, C.J. Brumlik, and C.R. Martin, *Chem. Mater.* 5, 902 (1993).
20. S.K. Chakarvarti and J. Vetter, *Micromech. Microeng* 3, 57 (1993).
21. S.P. Mondal, K. Das, A. Dhar, and S.K. Ray, *IOP Sci. Nanotechnol.* 18, 095606 (2007).
22. Y.D. Li, X.L. Li, R.R. He, J. Zhu, and Z. Deng, *J. Am. Chem. Soc.* 124, 1411 (2002).
23. T. Schmidt, K. Lischka, and W. Zulehner, *Phys. Rev.* B45, 8989 (1992).
24. J.H. Davies, *The Physics of Low-dimensional Semiconductors*, 2nd ed. (Science: Cambridge University Press, 1998), p. 8.
25. R. Kostic and D. Stojanovic, *Acta Phys. Pol. A* 4, 768 (2009).
26. R. Kostic and N. Romcevic, *Phys. Status Solidi C* 1, 2646 (2004).

Proceedings of the International Conference on Materials Science and Engineering, 2014

Growth and Characterization of CdS nanowires on ITO coated glass substrate

Shripriya Poduri[1,a] , Mitra Dutta[1,2,b], and Michael Stroscio[1,2,3,c]
[1] Department of Electrical and Computer Engineering, University of Illinois at Chicago, Chicago, IL 60607, USA
[2] Department of Physics, University of Illinois at Chicago, Chicago, IL 60607, USA.
[3] Department of Bioengineering, University of Illinois at Chicago, Chicago, IL 60607, USA
[a]spodur2@uic.edu, [b] dutta@uic.edu, [c]stroscio@uic.edu
* Shripriya Poduri

Keywords: CdS nanowire, anodic alumina matrix (AAM), vapor liquid solid (VLS) growth.

Abstract: Cadmium sulfide (CdS) nanowire (NW) arrays were prepared using two different processes: electrodeposition and vapor liquid solid (VLS) growth. In the first process, the nanowires were self assembled in the anodic alumina matrix (AAM) template deposited on an Indium Tin oxide (ITO) coated glass template by dc electrodeposition growth. On the other hand, in the second process, the nanowires were grown by VLS growth with gold (Au) nanoclusters acting as catalyst on ITO coated glass substrate. Energy dispersive X-ray spectroscopy studies on these nanowires confirm the growth of CdS nanowires on these substrates. Photoluminescence and Raman spectral studies were performed to study the electronic and vibrational properties of semiconductor nanowires. The photoluminescence spectra show green emission due to the presence of CdS nanowires and also strong 1 LO (longitudinal optical), 2 LO and 3 LO peaks were observed at 302, 603 and 906 cm^{-1} having an energy separation of 37 meV, demonstrating that the CdS nanowire had good crystalline properties.

Introduction:

Recently, nanowires and nanorods of metallic and semiconducting materials have generated a lot of interest because of their unique physical properties [1]. Nanowires have two quantum-confined dimensions and one unconfined dimension due to which these nanowires behave very differently than their bulk counterpart. Due to their high density of electronic states, diameter-dependent band gap, increased surface scattering of electrons and phonons, and high aspect ratio, semiconductor nanowires possess unique electrical, optical, and chemical properties compared to their bulk parent counterparts. These unique properties of nanowires make them very attractive for the applications of electronic devices, optical devices, and sensor devices etc [2-6]. CdS is a semiconducting material [7] with a direct band gap of about 2.5 eV which makes it suitable for many optoelectronic devices. One-dimensional CdS nanostructures are being used for a wide range of applications such as photoconductor [8], solar cell [9], photon emitters and lasers [10]. In recent years, these optoelectronic applications of CdS nanorods and thin films have generated a lot of interest and are widely being used owing to its excellent semiconducting properties.

Various nanowire growth methods like molecular beam epitaxy (MBE) [11], chemical vapor deposition [12], and physical vapor deposition have been reported for the fabrication of CdS nanowires, but growing of CdS nanowires in porous template such as anodic alumina membrane (AAM) is attractive because of its low cost, easy fabrication process and high throughput. The synthesis of CdS nanowires [13–15], nanotubes [16–19] and quantum dots [20] on porous alumina templates have been reported. It's best to grow nanowires in anodic alumina membranes (AAM) because of their large aspect ratio, easy fabrication and low cost. They are durable and can withstand high temperatures (up to 800 or 1000 ° C) [21], [22]. The length and diameter of the pores can also be controlled by changing the experimental conditions [21-25]. CdS nanowires were self assembled in an anodic alumina template of 200 nm thickness on indium tin oxide (ITO) coated glass by dc electrodeposition. Also, CdS nanowires were grown by VLS technique with Au nanoclusters as the catalyst on ITO coated glass substrate. Energy dispersive X-ray (EDS) analysis was performed to ascertain the growth of CdS nanowires. Photoluminescence (PL) and Raman spectral studies were performed on these substrates to probe electronic and vibrational properties of these grown nanowires.

Experimental details:

The ITO-coated 1"×1" glass substrates (1mm thick) were cleaned first in acetone and then in isopropanol by ultrasonicating them for 30 minutes to remove the organic residues. These substrates were then rinsed in deionized water and dried in dry air. A thin layer of aluminum (~200 nm thick) was deposited using e-beam evaporation. Prior to the deposition of aluminum, an interlayer of titanium of 5 nm thickness was grown using e-beam evaporation so as to prevent the poor connectivity between the ITO glass substrate and the aluminum layer and it also prevents the delamination of aluminum during anodization [26,27]. These templates were anodized at 40 V and 0.2 A in 0.3 M oxalic acid to produce well arranged hexagonal nanopores in the deposited aluminum layer. To remove the aluminum oxide layer and excess aluminum, the anodized template was heated in a mixture of phosphoric acid (5 wt. %) and chromic acid (10 wt. %) at 60 °C. The anodized template was again anodized at a potential of 40 V and 0.2 A in 0.3 M oxalic acid at 2-8 °C to obtain better and uniform nanopores because the pores grown during the first anodization step were poor and non uniform. The nanopores formed after the two step anodization in the template were of 10-60 nm in diameter and were very uniform. The pores were opened up after the two-step anodization, but also a barrier layer of oxide at the interface of the Al and Al_2O_3 was formed. The aluminum oxide barrier layer and non-uniformity in barrier layer thickness affects the growth and quality of the nanowires electrodeposited in the pores. The barrier layer prevents the filling of the CdS nanowires in the nanopores; hence this barrier layer has to be removed. It can be removed by immersing the substrate in 0.1 M phosphoric acid (H_3PO_4) for 30-40 minutes. Our CdS nanowires were grown via dc electrodeposition in AAM template on ITO coated glass substrate. The electrolyte used for CdS electrodeposition was 0.055 M $CdCl_2$ and 0.19 M elemental sulfur, dissolved in dimethyl sulfoxide (DMSO) [15, 16]. The temperature of the electrolyte was maintained at 120-150 °C and a constant current density of 2.5 mA/cm^2 was applied for 7-10 s with the deposition rate at 25-30 nm/s. After the electrodeposition, the samples were rinsed in hot DMSO followed by acetone and deionized water rinse. The CdS nanowires were liberated by dissolving the AAO templates in 1 M NaOH solution at room temperature for 8 min. However, after the two-step anodization, very uniform

pores of 10-60 nm appeared but it also grew with a barrier layer of oxide at the interface of the Al and Al_2O_3. This aluminum oxide barrier layer and non-uniformity in barrier layer thickness causes some problems such as affecting the growth and quality of the nanowires electrodeposited in the pores resulting in very little filling of nanowires in these pores. The barrier layer can be removed by dipping the substrate in 0.1M phosphoric acid (H_3PO_4) for 30-40 minutes. In this paper, CdS nanowires are cathodically deposited via dc electrodeposition. The electrolyte used for CdS electrodeposition was 0.055 M $CdCl_2$ and 0.19 M elemental sulfur, dissolved in dimethyl sulfoxide (DMSO) [28, 29]. The temperature of the electrolyte was maintained at 120-150 °C and a constant current density of 2.5 mA/cm^2 was applied for 7-10 s with the deposition rate at 25-30 nm/s [26]. After the electrodeposition, the samples were rinsed in hot DMSO followed by acetone and deionized water rinse. The CdS nanowires were liberated by dissolving the AAO templates in 1 M NaOH solution at room temperature for 8 min to be completely dissolved.

Additionally, CdS nanowires were grown using VLS technique with sputtered Au nanoclusters as catalyst. For VLS growth of nanowires, the ITO coated glass substrate were cleaned by soap water and then ultrasonicating them in acetone for 30 min followed by another 30 min ultrasonication in isopropanol and dried in nitrogen. Gold of 5 nm thickness was sputtered on these cleaned ITO glass substrate to catalyze the growth of nanowires. The CdS nanowires were synthesized in a quartz tube furnace with dual zone furnace heating instrument. CdS powder (~0.8 g, 99.999% pure, purchased from Sigma Aldrich) was placed in one heating zone and the ITO glass substrate with the sputtered gold nanoclusters in the second heating zone. 5% hydrogen was used as the transport gas with a flow rate of 100 sccm. The source and sample were heated to 900 and 580 °C, respectively for 1 h.

Finally, Field emission scanning electron microscopy imaging was done using JEOL 7500 FESEM to study the morphology and ascertain the growth of nanowires. Raman scattering and photoluminescence spectral studies were employed to investigate the longitudinal optical phonon modes and the electronic states of the CdS nanowires.

Results and Discussion:

Growing CdS nanowires in an AAM template is a difficult procedure due to the presence of a barrier layer of aluminum oxide which is difficult to etch out completely, thus causing non uniformities in the growth of nanowires and also the template should be free of cracks and defects [30, 31]. The elemental sulfur and $CdCl_2$ in the solution dissociates into S^{2-} ions and Cd^{2+} ions respectively. These S^{2-} ions react with Cd^{2+} ions to form CdS crystallites inside the nanopores of the template, thus forming the nanowires [32]. These crystallites nucleate on the walls of pores and gradually these pores get filled up with CdS crystallites forming nanowires [33]. The SEM images of the CdS nanowires grown after dc electrodeposition is shown in Figure 1.The diameter of the nanowires grown were approximately 10-25 nm.

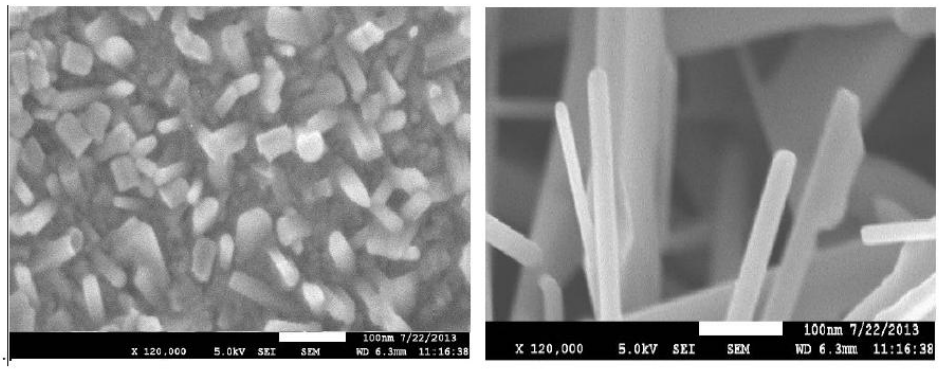

(a) (b)

Figure 1: (a) top view (b) side view SEM micrograph of CdS nanowires of 10-20 nm in diameter after annealing.

Energy Dispersive X-ray Spectroscopy EDS studies were done on these electrodeposited CdS nanowires and the results are shown in Figure 2.

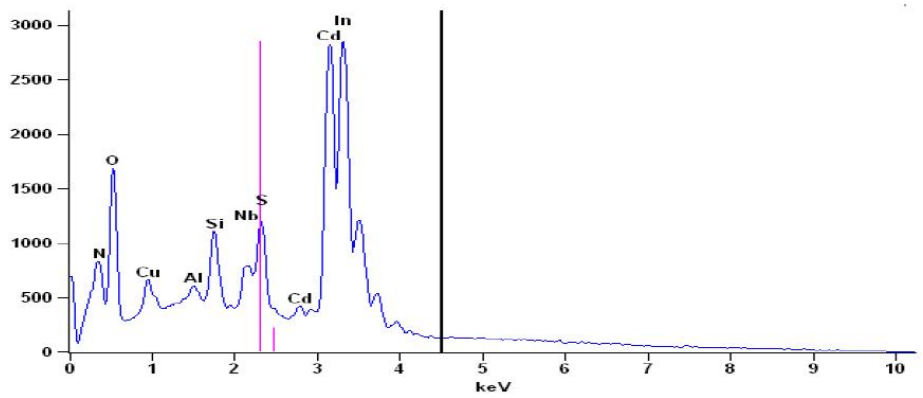

Figure 2: EDS of the CdS nanowires grown by electrodeposition.

Peaks of Cd and S in Figure 2 confirm the growth of CdS nanowires. Also, there were peaks of indium (In), oxygen (O), silicon (Si) due to the ITO coated glass substrate. Aluminum (Al) was also detected because there were some traces of aluminum left after the dissolution of alumina template in NaOH solution.

Furthermore, CdS nanowires were also grown using VLS growth mechanism. The ITO coated glass substrates were cleaned and sputtered with 5 nm of thickness of gold which serves as a catalyst for the growth of nanowire. CdS nanowires were grown in dual zone tube furnace having

CdS powder (~1g, 99.9% Sigma Aldrich) as source in one zone at 900 °C and the ITO coated glass with gold nanoclusters in the second zone at 580 °C for one hour and transport gas was 5% hydrogen with 95% argon. In the case of VLS growth, a small metal particle like Au which acts as a catalyst is deposited on the substrate and this forms a liquid/solid interface on heating. CdS vapor enters the liquid metal particle allowing it to become supersaturated resulting in CdS precipitation underneath the particle and thus forming a nanowire. The SEM images of these CdS nanowires by VLS growth is shown in Figure 3.

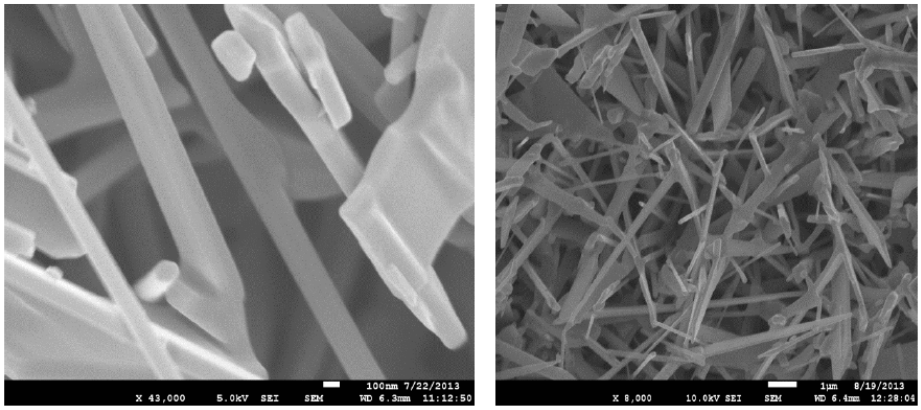

Figure 3: SEM images after the VLS growth of CdS nanowires.

To know the elemental composition of these samples Energy Dispersive X-ray Spectroscopy (EDS) were performed. The EDS result for the VLS grown nanowires are shown in Figure 4. Figure 4 shows that the Cd, S are present in the sample confirming the growth of CdS nanowires In and O are due to the ITO coating on the glass. Si is probably present because of the glass substrate.

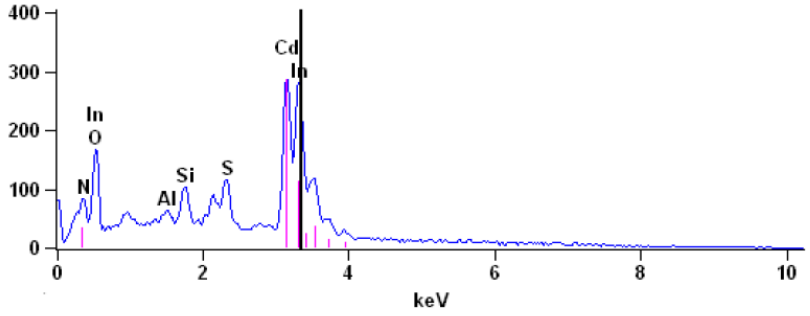

Figure 4: EDS result for VLS grown CdS nanowires.

Further studies like photoluminescence and Raman spectral studies were done to probe the electronic and optical properties of these nanowires. The photoluminescence characteristics of the grown CdS nanowires were investigated using a He–Cd laser of wavelength 325 nm for excitation at room temperature. The PL spectroscopy was performed on the electrodeposited CdS nanowires after dissolution of the AAO template in 1 M NaOH solution. The PL emission peak was observed at 506 nm (2.45 eV) for electrodeposited CdS nanowires and the peak for VLS grown nanowires was at 510 nm (2.43 eV) as shown in Figure 5 (a) and 5(b) respectively. The luminescence spectrum shows a strong green emission.

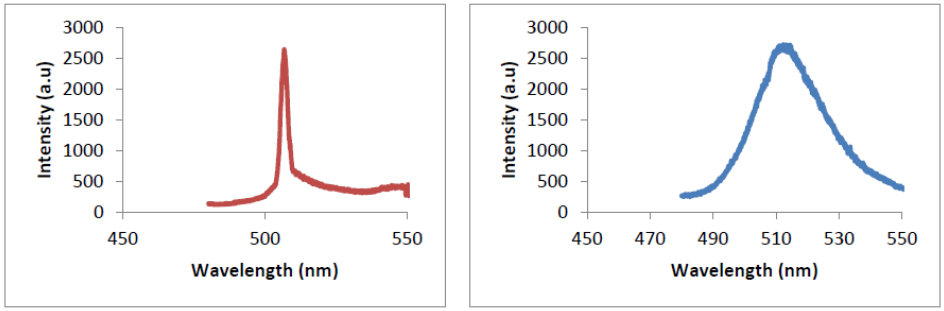

(a) (b)

Figure 5: (a) PL spectra for electrodeposited CdS nanowires with peak at 506 nm (b) PL spectra for VLS grown nanowires with peak at 510 nm.

The Raman spectrums were recorded using Ar^+ ion laser of 514 nm wavelength of these CdS nanowires. The Raman characteristics of these nanowires for VLS and electrodeposited nanowires are shown in Figure 6. Raman peaks were observed at 302 cm^{-1}, 603 cm^{-1} and 906 cm^{-1} corresponding to the longitudinal optical phonon (LO) modes 1LO, 2LO and 3LO, respectively, analogous to the peaks of pure CdS crystalline structure [12,34].

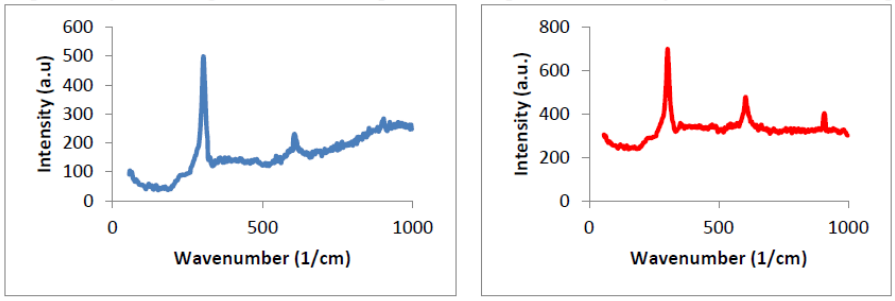

(a) (b)

Figure 6: Raman spectra of (a) electrodeposited CdS nanowires (b) VLS grown nanowires.

Strong 1LO, 2LO and 3LO peaks and the photoluminescence emission observed were in accordance with the phonons and the electronic band structure of the CdS material.

Conclusion:

CdS nanowires were grown using VLS growth and dc electrodeposition mechanism. It has been reported that the growth of CdS nanowires in porous alumina template via ac electrodeposition is the most efficient process due to the presence of barrier layer which cannot be completely removed. However we have employed dc electrodeposition for growing nanowires in a thin film (~200 nm thickness) of porous alumina template which is a quite difficult due to the thin film's susceptibility to crack and the poor connectivity to the ITO coated glass substrate. CdS nanowires were also grown using VLS growth mechanism to compare the results with the electrodeposition growth of CdS nanowires in a template. The Raman and luminescence spectrum of the CdS nanowires grown by electrodeposition and VLS mechanism show good crystallinity of CdS nanowires.

Acknowledgement:

This research was supported in part by the AFOSR.

References

[1] J.R. Heath, P.J. Kuekes, G. Snyder, R.S. Williams, Science 280 (1998) 1717-1719.
[2] Tonucci R J, Justus B L, Campillo A J and Ford C E, Science 258 (1992) 783-785.
[3] R. Agarwal, C. J. Barrelet, and C. M. Lieber, Nano Lett. 5 (2005) 917-923.
[4] X. Duan, Y. Huang, Y. Cui, J. Wang, and C. M. Lieber, Nature London 409 (2001) 66-72.
[5] M. T. Borgstrom, V. Zwiller, E. Muller, and A. Imamoglu, Nano Lett. 5 (2005) 1439-1443
[6] X. Duan, Y. Huang, R. Agarwal, and C. M. Lieber, Nature London 421(2003) 241-246
[7] A. R. Hutson, Phys. Rev. Lett. 4 (1960) 505-507.
[8] T. Gao, Q. H. Li, and T. H. Wang, Appl. Phys. Lett. 86 (2005) 173105-108.
[9] Y. Kang and D. Kim, Sol. Energy Mater. Sol. Cells 90 (2006) 166-174.
[10] X. Duan, Y. Huang, R. Agarwal, and C. M. Lieber, Nature London 421, (2003) 241-245.
[11] KobayashiM, Nakamura S, Kitamura K, Umeya H, Jia A, Yoshikawa A, Shimotomai M and Kato Y, J. Vac. Sci.Technol. B 17 (2005) 1999-2002.
[12] Abdi A, Titova L V, Smith L M, Jackson H E, Yarrison-Rice J M and Lauhon, J L Appl. Phys. Lett. 88 (2006) 043118.
[13] Routkevitch D, Bigioni T, Moskovits M and Xu, J. Phys. Chem. 100 (1996) 14037-047.
[14] Xu D, Chen D, Xu Y, Shi X, Guo G, Gui L and Tang Y, Pure Appl. Chem. 72 (2000) 127-130.
[15] Cao H, Xu Y, Hong J, Liu H, Yin G, Li B, Tie C and Xu Z, Adv. Mater. 13 (2001) 1393 - 1397.
[16] Zhang H, Ma X, Xu J and Yang D, J. Cryst. Growth 263 (2004) 372-376.

[17] Zhang H, Ma X, Xu J, Niu J, Sha J and Yang D, J. Cryst. Growth 246 (2002) 108-111.
[18] Shen X P, Yuan A H, Wang F, Hong J M and Xu Z, Solid State Commun. 133(2005) 19-25.
[19] Nia Y, Mab X, Hongb J and Xua Z, Mater. Lett. 58 (2004) 2754-2758
[20] S Bandyopadhyay, A E Miller, H C Chang, G Banerjee, V Yuzhakov, D-F Yue, R E Ricker, S Jones, J A Eastman, E Baugher and M Chandrasekhar, IOPScience Nanotechnology **7** (1996) 360-371.
[21] J. Sarkar, G. G. Khan, and A. Basumallick, Bull. Mater. Sci. 30 (3) (2007) 271-290.
[22] A. L. Friedman and L. Menon. J. Elec. Soc. 154 (4) (2007) E68-E70.
[23] Kong, Kong, J., Franklin, N., Zhou, C.,Chapline M., Peng S., Cho K., Dai H., Science, 287 (2000) 622-28.
[24] Nevin Tasaltın, Sadullah Ozturk Necmettin Kılınc¸, Hayrettin Yuzer, Zafer Ziya Ozturk, Nanoscale Res Lett 5 (2010) 1137–1143.
[25] L. Menon, S. Bandyopadhyay and H. Nalwa, "Chapter: Synthesis of Nanowires using Porous Alumina" American Scientific Publishers, 142-191,2003.
[26] Piao Liu, Vijay P Singh, Suresh Rajaputra, IOPscience Nanotechnology 21 (2010) 115303.
[27] Thelese R. B. Foong , Alan Sellinger and Xiao Hu, ACS Nano Lett.11 (2008) 2250-56.
[28] Dongsheng Xu, Yajie Xu, Dapeng Chen, Guolin Guo, Linlin Gui, Youqi Tang, J. of Chemical Physics Letters 325 (2000) 340–344.
[29] Yang Y, Chen H, Mei Y, Chen J, Wu X and Bao X, Solid State Commun.123 (2002) 279-82.
[30] Klein, J. D., Herrick, R. D., Palmer, D.Sailor, M. J., Brumlik, C. J., Martin, C. R., Chem. Mater. 5 (1993), 902-907.
[31] Chakarvarti, S. K.; Vetter, J. Micromech. Microeng 3 (1993) 57-60.
[32] S P Mondal, K Das, A Dhar and S K Ray, IOPscinece Nanotechnology 18 (2007) 095606.
[33] Li Y D, Li X L, He R R, Zhu J, Deng Z X, Li Y D, Li X L, He R R, Zhu J and Deng Z X J. Am. Chem. Soc.124 (2002) 1411-15.
[34] Kostic R and Romcevic N, J. of Phys. Stat. Sol. (c) 1 11(2004) 2646-49.

Section III: Plasmonic Effects in Nanostructures

Journal of ELECTRONIC MATERIALS, Vol. 43, No. 3, 2014
DOI: 10.1007/s11664-013-2924-1

Strong Enhancement of Near-Band-Edge Photoluminescence of ZnO Nanowires Decorated with Sputtered Metallic Nanoparticles

MOHSEN PURAHMAD,[1,2] MICHAEL A. STROSCIO,[1,3] and MITRA DUTTA[1,4]

1.—Department of Electrical and Computer Engineering, University of Illinois at Chicago, Chicago, IL 60607 , USA . 2.—e-mail: mpurah2@uic.edu. 3.—e-mail: stroscio@uic.edu. 4.—e-mail: dutta@uic.edu

The effect of the Ar plasma during metal deposition on the photoluminescence (PL) of metal-coated ZnO nanowires (NWs) has been investigated. Strong enhancement of near-band-edge emission (NBE) is observed for ZnO NWs coated with Al and Ni nanoparticles (NPs) by radiofrequency magnetron sputtering, while the samples coated with NPs by e-beam evaporation show quenching of the PL intensity. A model is proposed that satisfies the observed experimental results and assigns the strong enhancement of the NBE PL of ZnO NWs to excitons bound to structural defects in the surface layer of the ZnO NWs.

Key words: Photoluminescence, zinc oxide nanowires, surface traps, sputtering

INTRODUCTION

Zinc oxide (ZnO) is a II–VI compound semiconductor with a wide direct bandgap (3.37 eV), large exciton binding energy (60 meV), and stable thermal and mechanical properties, making it a promising candidate for optoelectronic applications such as short-wavelength semiconductor lasers and light-emitting diodes.[1–3] ZnO nanowires (NWs) have additional functionality arising from their size which allows for further flexibility in bandgap engineering. Since ZnO NWs have weak near-band-edge emission (NBE), numerous studies have been carried out to enhance the NBE and photoluminescence (PL) efficiency of ZnO NWs. Different methods such as polymer coating of ZnO NWs[4,5] and hydrogen plasma treatment[6] are seen to boost the NBE and PL efficiency of ZnO NWs. Recently, the effect of metallic nanoparticles (NPs) on the PL properties of ZnO NWs has been the focus of much research.[3,7] In most studies an enhancement of NBE was observed and the results were interpreted in terms of surface plasmons,[8] unintentional hydrogen incorporation,[9] and the nature of the contact formed between the metal and ZnO NWs.[7] In this work we investigated the effect of the presence of Ar plasma during metallic NP deposition on the PL intensity of ZnO NWs. A strong enhancement of the NBE and a relative reduction of visible emission from the gap are seen for ZnO NWs on which metallic NPs were sputtered. By considering the nature of the contact formed between the ZnO NWs and metallic NPs, the concentration of ambient hydrogen during metal sputtering, and comparison of the PL intensities from ZnO NWs with NPs deposited by sputtering versus e-beam evaporation, a model is proposed that satisfies the observed strong enhancement of NBE and related reduction of the visible peak.

(Received May 28, 2013; accepted November 20, 2013; published online December 25, 2013)

EXPERIMENTAL PROCEDURES

ZnO NWs were grown by the vapor–liquid–solid method in a horizontal quartz tube at atmospheric pressure on *n*-type, 100-plane silicon wafer as substrate. Previously, the substrates were cleaned using acetone and dried in a nitrogen stream, then coated with a 3-nm layer of gold thin film using

e-beam evaporation. ZnO powder (99.99%; Sigma-Aldrich Company, USA) mixed with graphite (powder <20 μm; Sigma-Aldrich Company, USA) at weight ratio of 1:1 was used to carry out the carbothermal reaction process. The coated substrates and ceramic boat with the ZnO and graphite powders were placed in the middle of a 2-inch quartz tube. The system was heated to 900°C to 910°C with a constant (350 sccm) flow of Ar for 30 min to 50 min, then cooled down to room temperature. The grown ZnO NWs were characterized using a variable-pressure Hitachi S-3000N scanning electron microscope (SEM) and x-ray photoelectron spectroscopy (XPS). Figure 1a shows SEM images of as-grown ZnO NWs with average length of about 20 μm and diameter in the range of 50 nm to 200 nm. Aluminum (Al) and nickel (Ni) metal NPs were deposited on the ZnO NWs using a radiofrequency (RF) magnetron system with the corresponding metal target at room temperature. A schematic diagram of the RF magnetron system used for decorating the ZnO NWs is shown in Fig. 2. For all samples, before starting the plasma and metal deposition, the experimental chamber was pumped down to a high vacuum ($\sim 10^{-6}$ Torr) and the sputtering process was carried out under a constant (45 sccm) flow of ultrapure Ar at power of 100 W. XPS spectra of as-grown ZnO NWs and coated ZnO NWs measured using a Kratos AXIS-165 spectrometer are shown in Fig. 1b. Transmission electron microscopy (TEM) images of as-grown ZnO NWs and of ZnO NWs coated with Al NPs are shown in Fig. 1c and d. As seen in Fig. 1d, the metallic NPs have an island-like morphology consisting of a network of sputtered metallic NPs on the surface of ZnO NW. Room-temperature PL was excited using a 325-nm HeCd laser, and the PL emission was collected using an Acton 2500i spectrometer. Low-temperature PL measurements were performed in a closed-cycle helium cryostat at 8.5 K.

RESULTS AND DISCUSSION

Room-temperature PL spectra of as-grown ZnO NWs and of those coated with RF magnetron sputtered Al and Ni NPs are compared in Fig. 3a, b. The contacts between the semiconductor and metal will induce bending of the energy band of the semiconductor at the interface. It is also well known that the PL spectra of ZnO NWs mainly reflect their energy band information at the NW surface. Hence, it is anticipated that the type of junction between the deposited metals and the ZnO NWs will result in a change of their PL properties.[7] Strong enhancement of NBE is seen for both ZnO NWs decorated with Al and Ni NPs. Since the junction between ZnO NW

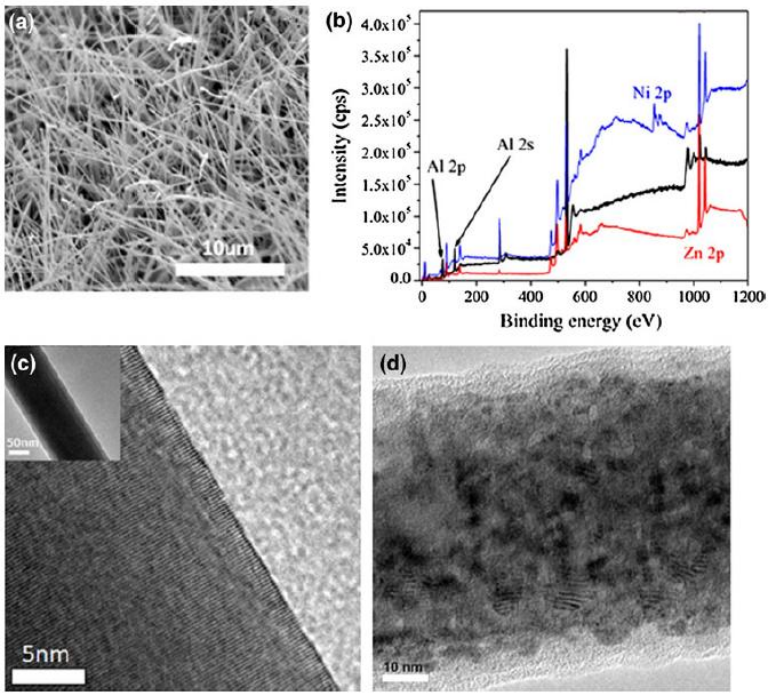

Fig. 1. (a) SEM image of as-grown ZnO NWs. (b) XPS spectra of as-grown ZnO NWs (red), Ni-coated ZnO NWs (blue), and Al-coated ZnO NWs (black). (c) TEM images of as-grown ZnO NW and (d) Al-coated ZnO NW (Color figure online).

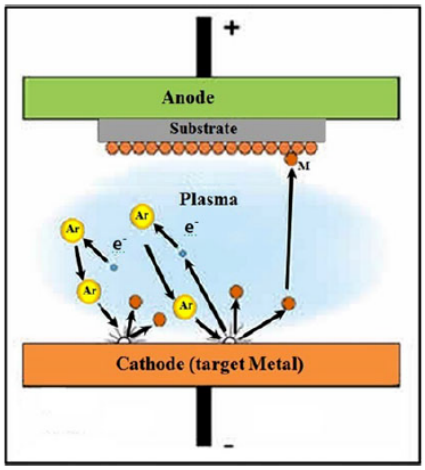

Fig. 2. Schematic diagram of the RF magnetron system.

and Al is an ohmic contact and the junction between the Ni and ZnO NW is a Schottky contact,[7] the experimental results shown in Fig. 3a, b demonstrate that this strong enhancement of NBE is not mainly due to the nature of the contact formed between the metallic NPs and ZnO NWs. However, the type of contact formed between the ZnO and metallic NPs may have a small effect as a higher enhancement ratio of NBE is seen in the case of ZnO NWs decorated with Al NPs.

In addition to the increase in intensity of the NBE peak, we also see a related reduction of the visible peak, as shown in Fig. 3a, b. The room-temperature and low-temperature (8.5 K) PL spectra of as-grown ZnO and after sputtering with Al NPs for a shorter sputtering time (90 s) are presented in Fig. 4a, b, where the first emission peak in Fig. 4b can be assigned to the free exciton (FX) at 367.6 nm (3.372 eV)[4,10] and the second peak at 368.5 nm (3.364 eV) is due to the surface-excitonic emission band (SX).[10] On the low-energy side, contributions from the recombination of excitons bound to neutral donors (DX) are observed at 3.69 nm (3.359 eV)[10] and defects located in the NWs (A-line) give rise to a PL peak at 373.5 nm (3.319 eV). Finally, the PL peak located at 382.45 nm (3.242 eV) comes from the first-order longitudinal phonon replica of A-line.[7,11] As presented in Fig. 4b, the strong enhancement of NBE is mostly related to SX peak enhancement. Temperature-dependent PL spectra of as-grown ZnO NWs and Al-sputtered NWs are shown in Fig. 4c and d, and the inset figure shows the peak energy versus temperature. The PL transitions are dominated by excitons bound to neutral donors at low temperatures, with a very small free exciton peak visible. As the temperature increases, the free exciton thermalizes and cannot be seen at

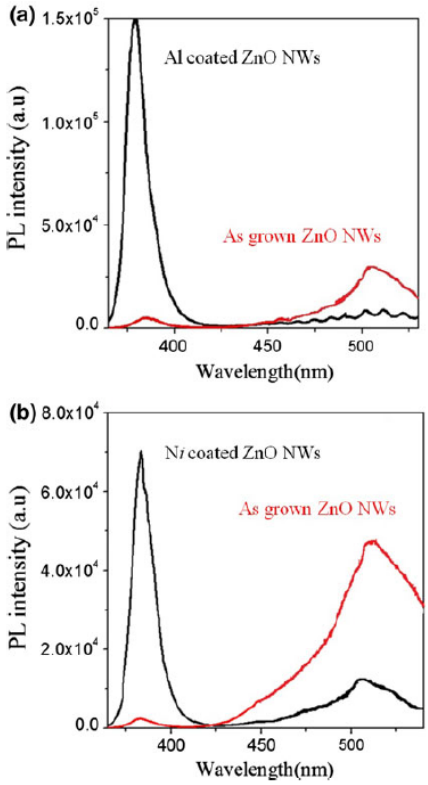

Fig. 3. (a) Room-temperature PL spectrum of as-grown ZnO NWs (red) and PL spectrum of ZnO NWs coated with Al NPs for 120 s (black). (b) Room-temperature PL spectrum of as-grown ZnO NWs (red) and PL spectrum of ZnO NWs coated with Ni NPs for 120 s (black) (Color figure online).

higher temperature. It can be observed that all peaks systematically shift to lower energy with increasing temperature. The temperature dependence of the PL intensity can be expressed by the Arrhenius expression:[12]

$$I(T) = \frac{I_0}{1 + A\exp\left(\frac{-E}{K_B T}\right)}, \quad (1)$$

where ΔE is the activation energy of the thermal quenching process, K_B is the Boltzmann constant, I_0 is the emission intensity at 0 K, T is the thermodynamic temperature, and A is a constant. The dependence of the integrated PL intensity of the ultraviolet (UV) band on temperature is shown in Fig. 4e. By fitting the PL spectra using the Arrhenius expression, the activation energy of SX was obtained as 17.32 meV for as-grown ZnO NWs and 14.47 meV for ZnO NWs decorated with sputtered metallic NPs, in reasonable agreement with reported values.[10,13]

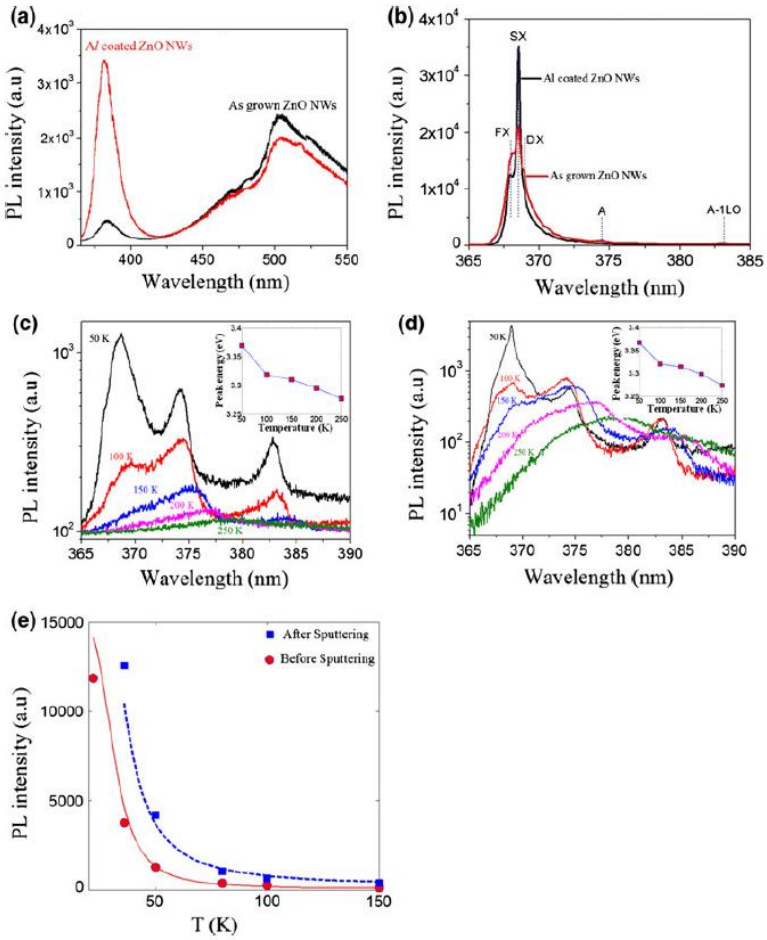

Fig. 4. (a) Room-temperature PL spectra of as-grown ZnO NWs and Al-sputtered (90 s) ZnO NWs. (b) PL spectra of as-grown ZnO NWs and Al-sputtered NWs at 8.5 K. Temperature-dependent PL spectra (near-UV region) of (c) as-grown ZnO NWs and (d) Al-sputtered ZnO NWs; insets show SX peak energy versus temperature. (e) Integrated intensity of the neutral donor-bound exciton of ZnO NWs as a function of temperature with theoretical fitting curve.

To investigate the effect of metallic NPs unexposed to Ar plasma, the PL from ZnO NWs coated with e-beam-evaporated Al NPs was studied. The PL spectra of ZnO NWs before and after e-beam Al evaporation for different deposition times are illustrated in Fig. 5, showing quenching of the NBE which may be due to the formation of metal-induced gap states on the NW surface layer.[14]

It has been reported that, when ZnO NWs are coated with a thin layer of metal, a large number of additional states within the bandgap will be introduced.[14] These additional defects in the surface region will result in a higher trapping rate of electrons, therefore reducing the rate of excitonic recombination in the surface layer. As seen in Fig. 5, e-beam-evaporated Al thin film on ZnO NWs resulted in a relative quenching of the NBE peak.[14]

In the case of one-dimensional systems such as ZnO NWs, where the ratio of surface area to volume is high, surface defects, near-surface traps, and surface-adsorbed species such as O_2 molecules and OH^- offer alternative pathways for deexcitation of photoexcited carriers and play a significant role in

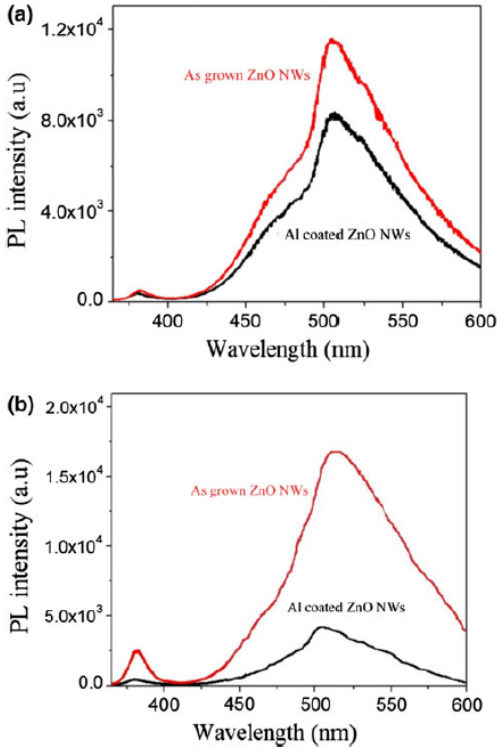

Fig. 5. Room-temperature PL spectra of as-grown ZnO NWs (red) and ZnO NWs coated with Al NPs by e-beam evaporation (black) for different evaporation times: (a) 60 s and (b) 120 s (Color figure online).

the carrier relaxation dynamics.[15,16] Typically, the O_2 molecule, one of the most common adsorbates on the surface of ZnO NWs, undergoes chemisorption onto the NW surface by capturing a free electron from the *n*-type ZnO in an oxidizing ambient as shown in Eq. (2).[15–18]

$$O_2(g) + e^- = O_2^-(ad) \quad (2)$$

It is well known that intrinsic defects such as oxygen vacancies in as-grown ZnO NWs can be reduced by O_2 or Ar annealing, resulting in a relative quenching of the visible emission peak whereas the NBE peak is not changed in O_2- or Ar-annealed ZnO NWs.[19,20] However, the focus of this study is the reduction of surface defects and traps not intrinsic defects.

At the growth temperature of 900°C and atmospheric pressure, a major part of the species adsorbed on the surface of ZnO NWs will be O_2^-, which acts as a surface trap. Upon illumination, some photoexcited carriers will migrate to these surface traps. As shown in Fig. 6, a part of the

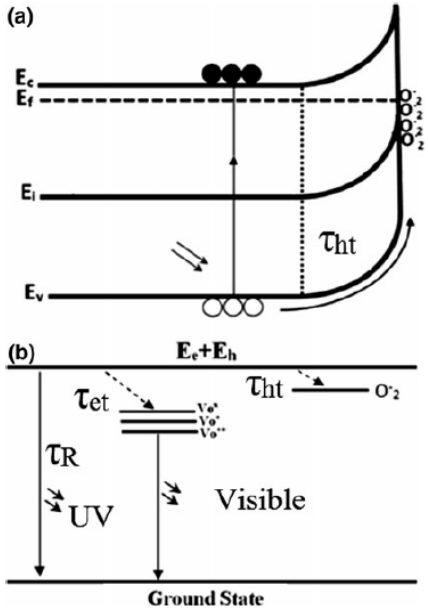

Fig. 6. (a) Schematic diagram of the band bending of ZnO NWs. (b) Corresponding phenomenological model of the trapping pathways.

photoexcited holes are trapped by the adsorbed oxygen species on the NW surface[15] and other photoexcited carriers are trapped by point defects such as oxygen vacancies and are believed to be the origin of the visible emission peak in the PL spectrum of ZnO NWs.[13] It is well known that the PL emission band at about 3.367 eV has its origin in the surface region of ZnO NWs,[5,10] and with decreasing wire diameter its relative contribution to the NBE increases continuously.[10] Hence, fewer screened surface trapping sites lead to a lower density of separated electrons and holes in the surface region, which results in a higher density of excitons near the NW surface. So, surface cleaning of ZnO NWs from the trapping sites results in an increase of the SX band intensity.[5] The relative reduction of visible emission seen in ZnO NWs decorated with sputtered metallic NPs can also be attributed to the trapping sites at the NW surface.

Oxygen vacancies are believed to be the origin of the visible emission peak in the PL spectrum of ZnO NWs,[13] and the mechanism of the visible emission peak with a maximum at 2.45 eV originates from single positively charged oxygen vacancies (V_O^+) located within the ZnO NW. Three different types of oxygen vacancy can occur in ZnO NWs: doubly ionized oxygen vacancies V_O^{++}, singly ionized oxygen vacancies V_O^+, and neutral oxygen vacancies V_O^x, as shown in Fig. 6b.[13] These vacancies need to be activated by a hole. So, the activation process

requires photoexcited holes which are trapped at the surface. Then, the holes may tunnel into the deep-level defects to create optically active oxygen vacancies.[5] This model is based on the assumption that surface-related processes are dominant for ZnO NWs.[5] Trapping sites such as O^{2-}, O^{-} or OH^{-} located at the NW surface lead to separation of electron–hole pairs in this region. Then, the holes will be captured at the surface traps. By cleaning the surface of ZnO NWs from trapping sites, fewer holes are able to be captured at surface traps, which quenches the visible emission peak.[5]

The experimental results demonstrate that decorating ZnO NWs with metal NPs in the presence of high-energy Ar atoms cleans the surface of ZnO NWs from near-surface traps and surface-adsorbed species, thus leading to strong enhancement of NBE and a relative reduction of the visible peak. Comparison of the room-temperature PL spectra shown in Figs. 3a and 4a also shows that increasing the sputtering time can lead to better surface cleaning and therefore stronger enhancement of NBE.

It has also been reported that hydrogen atoms can act as shallow donors and occupy interstitial sites in addition to oxygen vacancies, which can result in enhancement of NBE and quenching of the visible emission peak.[6,21] However, since the metal deposition was performed in high vacuum (10^{-6} Torr) before starting the plasma, and ultrapure Ar was used, it is expected that the presence of hydrogen is negligible during the sputtering process and the strong enhancement of the NBE and quenching of the visible peak cannot be because of hydrogen incorporation.

CONCLUSIONS

Room- and low-temperature PL spectra of as-grown ZnO NWs and those coated with metallic NPs using different deposition methods were investigated. It was shown that the PL spectra of ZnO NWs coated with sputtered metallic NPs demonstrate strong enhancement of the NBE peak and a relative reduction of the visible peak. Effects of the type of contact formed between the metallic NPs and ZnO NWs and unintentional hydrogen incorporation have been investigated. The observed experimental results reveal that decorating ZnO NWs with metal NPs in the presence of high-energy Ar atoms can decrease nonradiative relaxation pathways and lead to strong enhancement of NBE and a relative reduction of the visible peak.

REFERENCES

1. A.P. Abiyasa, S.F. Yu, S.P. Lau, E.S.P. Leong, and H.Y. Yang, *Appl. Phys. Lett.* 90, 231106 (2007).
2. H. Zhu, C.X. Shan, B.H. Li, Z.Z. Zhang, D.Z. Shen, and K.L. Choy, *J. Mater. Chem.* 21, 2848 (2011).
3. T. Chen, G.Z. Xing, H.Y. Chen, and T. Wu, *IOP J. Nanotechnol.* 19, 435711 (2008).
4. K.W. Liu, R. Chen, G.Z. Xing, T. Wu, and H.D. Sun, *Appl. Phys. Lett.* 96, 023111 (2010).
5. J.P. Richters, T. Voss, L. Wischmeier, I. Ruckmann, and J. Gutowski, *Appl. Phys. Lett.* 92, 011103 (2008).
6. Y. Li, R. Uchino, T. Tokizono, A. Paulsen, M. Zhong, M. Shuzo, I. Yamada, and J. Delaunay, *Mater. Res. Soc. Symp. Proc.* 1206, 03 (2010).
7. Y.J. Fang, J. Sha, Z.L. Wang, Y.T. Wan, W.W. Xia, and Y.W. Wang, *Appl. Phys. Lett.* 98, 033103 (2011).
8. Wei Tang, Dongliang Huang, Wu Lili, Chaozhong Zhao, Xu Lingling, Hong Gao, Xitian Zhang, and Weibo Wan, *CrystEngComm* 13, 2336 (2011).
9. A. Dev, J.P. Richters, J. Sartor, H. Kalt, J. Gutowski, and T. Voss, *Appl. Phys. Lett.* 98, 131111 (2011).
10. L. Wischmeier, T. Voss, I. Ruckmann, and J. Gutowski, *IOP J. Nanotechnol.* 19, 135705 (2008).
11. C. Bekeny, T. Voss, B. Hilker, and J. Gutowski, *Appl. Phys. Lett.* 102, 044908 (2007).
12. H.C. Hsu, C.S. Cheng, C.C. Chang, S. Yang, C.S. Chang, and W.F. Hsieh, *IOP J. Nanotechnol.* 16, 297 (2005).
13. Z.M. Liao, H.Z. Zhang, Y.B. Zhou, J. Xu, J.M. Zhang, and D.P. Yu, *J. Phys. Lett. A* 372, 4505 (2008).
14. J. Richters, A. Dev, S. Müller, R. Niepelt, C. Borschel, C. Ronning, and T. Voss, *Phys. Status Solidi RRL* 3, 166 (2009).
15. M. Li, G. Xing, L. Foong Nien Ah Qune, G. Xing, T. Wu, C. Hon Alfred Huan, X. Zhang, and T.C. Sum, *Phys. Chem. Chem. Phys.* 14, 3075 (2012).
16. W.Z. Liu, H.Y. Xu, J.G. Ma, C.Y. Liu, Y.X. Liu, and Y.C. Liu, *Appl. Phys. Lett.* 100, 203101 (2012).
17. C. Soci, A. Zhang, B. Xiang, S.A. Dayeh, D.P.R. Aplin, J. Park, X.Y. Bao, Y.H. Lo, and D. Wang, *Nano Lett.* 7, 1003 (2007).
18. Y. Li, F.D. Valle, M. Simonnet, I. Yamada, and J.J. Delaunay, *Appl. Phys. Lett.* 94, 023110 (2009).
19. B. Ha, H. Ham, and C.J. Lee, *J. Phys. Chem. Solids* 69, 2453 (2008).
20. J.H. He, C.S. Lao, L.J. Chen, D. Davidovic, and Z.L. Wang, *J. Am. Chem. Soc.* 127, 16376 (2005).
21. X. Liu, X. Wu, H. Cao, and R.P.H. Chang, *J. Appl. Phys.* 95, 3141 (2004).

Section IV: Phonon Engineering in Graphene-based Nanostructures

Superlattices and Microstructures 46 (2009) 881–888

Contents lists available at ScienceDirect

Superlattices and Microstructures

journal homepage: www.elsevier.com/locate/superlattices

Quantized long-wavelength optical phonon modes in graphene nanoribbon in the elastic continuum model

Jun Qian [a], Matthew J. Allen [b], Yang Yang [c], Mitra Dutta [a,d], Michael A. Stroscio [a,d,e,*]

[a] Department of Electrical and Computer Engineering, University of Illinois at Chicago, Chicago, IL 60607, USA

[b] Department of Chemistry, University of California, Los Angeles, CA 90095, USA

[c] Department of Materials Science and Engineering and California NanoSystems Institute, University of California, Los Angeles, CA 90095, USA

[d] Department of Physics, University of Illinois at Chicago, Chicago, IL 60607, USA

[e] Department of Bioengineering, University of Illinois at Chicago, Chicago, IL 60607, USA

ARTICLE INFO

Article history:
Received 17 July 2009
Received in revised form
25 August 2009
Accepted 2 September 2009
Available online 18 September 2009

Keywords:
Graphene nanoribbon
Confined optical phonon
Elastic continuum model
Deformation potential

ABSTRACT

This paper presents an analytical displacements and dispersion relations for optical phonons of a graphene sheet. These results are used to derive the optical deformation potential interactions for graphene as well as to obtain descriptions of the confined optical phonons for graphene.

1. Introduction

Graphene has attracted a great deal of attention since it was first successfully made by Geim [1,2] for its unique electronic, magnetic and thermal properties [3–8]. Carrier-phonon scattering will affect the electrical properties of graphene, such as resistivity and Fermi level shift [9–13]. It is important to study both the acoustic and optical phonons in graphene. Phonon dispersion has been studied by Raman and neutron scattering in graphite [14–16] and

* Corresponding author at: Department of Electrical and Computer Engineering, University of Illinois at Chicago, Chicago, IL 60607, USA.
E-mail address: stroscio@uic.edu (M.A. Stroscio).

0749-6036/$ – see front matter © 2009 Elsevier Ltd. All rights reserved.
doi:10.1016/j.spmi.2009.09.001

J Comput Electron (2012) 11:293–301
DOI 10.1007/s10825-012-0400-4

Phonon bottleneck effects in rectangular graphene quantum dots

Jun Qian · Mitra Dutta · Michael A. Stroscio

Published online: 31 March 2012

Abstract For a graphene sheet with confining structures in the orthogonal directions of zigzag- and armchair-edge, the confined carrier states are determined. These wavefunctions and eigenvalues are used to study carrier-longitudinal optical (LO)-phonon interactions in these graphene quantum dots. The optical deformation potential is derived for these graphene quantum dots as the basis for the study of these carrier-LO-phonon interactions. Phonon bottleneck effects are identified and the Fermi golden rule transition rates are formulated.

Keywords Graphene · Quantum dots · Confined phonons

1 Introduction

Graphene [1, 2], a plane of sp^2-bonded carbon atoms arranged in honeycomb lattices, has attracted vast attention for its unique electronic properties [3–7]. The nanostructures based on graphene, such as nanoribbons [4, 8–10] and quantum dots [11–13], have been considered as important building blocks for future nanoelectronic devices. The electronic properties of graphene nanostructures strongly depend on the confined dimensions [4, 10, 13]. The effective-mass approximation is widely used to study the electronic states and the transport properties of the carbon based nanomaterials, such as carbon nanotube [14, 15], bulk graphene [5, 15] and graphene nanoribbons [6, 8]. At room temperature carrier-phonon scattering is the dominating source of the resistivity in moderately doped graphene based nanostructures [10, 16]. The long wavelength optical phonons, which dominate for high-energy carrier states [10, 17], can be described well by elastic continuum models in both carbon nanotubes and graphene [14, 18–21]. Confined optical phonon modes need to be carefully considered, especially in confined dimensions [22–24]. Thus, it is essential to consider double quantization effects for both electrons and phonons during the scattering process in each confined dimension of a graphene structure.

In this paper, we study the electronic states, the optical phonon modes and the electron-longitudinal optical (LO) phonon interactions in a two dimensional (2D) confined graphene nanosheet having orthogonal zigzag (ZZ)-edge and armchair (AC)-edge, i.e. rectangular graphene quantum dot (RGQD). The extreme quantum limit is considered for these as that infinite barriers are assumed at the boundaries, as shown in Fig. 1.

Using the effective mass method [8, 15] we describe the discrete electronic states near the K and K′ Dirac point with the adoption of hard wall boundary conditions [10]. The normalized optical phonon modes in RGQDs are calculated using the elastic continuum model similar to our previous calculation in graphene nanoribbons [22]. The phonon bottleneck effect, which is very common in three-dimensional confined quantum dots [25], is found to exist in most cases of RGQDs. As will be shown, the carrier-LO phonon scattering, which generally dominates in bulk graphene or graphene nanoribbons at room temperature

J. Qian · M. Dutta · M.A. Stroscio (✉)
Department of Electrical and Computer Engineering, University of Illinois at Chicago, Chicago, IL 60607, USA
e-mail: stroscio@uic.edu

M. Dutta · M.A. Stroscio
Department of Physics, University of Illinois at Chicago, Chicago, IL 60607, USA

M.A. Stroscio
Department of Bioengineering, University of Illinois at Chicago, Chicago, IL 60607, USA

Section V: Phonon Engineering in Nanowires --- Piezoelectric Interactions

JOURNAL OF APPLIED PHYSICS 111, 054514 (2012)

Piezoelectricity in zincblende polar semiconductor nanowires: A theoretical study

Banani Sen,[a] Michael Stroscio,[b] and Mitra Dutta[c]
Department of Electrical and Computer Engineering, University of Illinois at Chicago, Chicago, Illinois 60607, USA

(Received 23 January 2012; accepted 11 February 2012; published online 14 March 2012)

A systematic evaluation of the piezoelectrically induced electric polarization vector and the associated potential on the application of mechanical strain to charge-free semiconductor nanowires with zincblende crystal structure is reported. It is found that the bending mode which is easier to realize in practice over stable compressional modes generates maximum piezo energy for these zincblende semiconductor nanowires. Also zincblende ZnO nanowires are found to be superior over zincblende AlN and GaN wires for piezo energy harvesting. © *2012 American Institute of Physics*. [http://dx.doi.org/10.1063/1.3692604]

I. INTRODUCTION

Energy harvesting has been around for centuries in the form of windmills, watermills, and passive solar power systems. The current frontier of energy harvesting is an array of micro-scale technologies that scavenge milliwatts from solar, vibrational, thermal, and biological sources; of which vibration-based mechanical energy is the most ubiquitous and accessible source of energy.[1,2] Over the last decade much research has been focused on nanodevices based on nanoscale piezoelectric components to harvest energy on micro-/nano-scale.[3,4] However, the physics behind the electromechanical phenomena in semiconductors are still poorly studied. On application of an external strain to a piezoelectric crystal, macroscopic polarization depending on the intrinsic properties of the crystal is produced as a result of the displacements of ions. In view of this interest, this article provides a detailed treatment of the piezoelectric effect in zincblende nanowires based on the full piezoelectric tensor.

II. THEORY

In order to determine the piezoelectric polarization in a zincblende material it is necessary to consider the piezoelectric tensor of the material under consideration and to determine the strain components corresponding to the deformation under consideration. The piezoelectric tensor relating the piezoelectric polarization vector and the acoustic strain vector may be expressed in matrix notation for the case of a zincblende crystal in Cartesian coordinates as

$$\bar{e} = \begin{pmatrix} 0 & 0 & 0 & e_{x4} & 0 & 0 \\ 0 & 0 & 0 & 0 & e_{x4} & 0 \\ 0 & 0 & 0 & 0 & 0 & e_{x4} \end{pmatrix}. \quad (1)$$

For the case of uniform plane wave propagation at an arbitrary angle η in the XZ plane of a zincblende crystal the piezoelectric stress matrix transforms as

$$\bar{e'} = [a][\bar{e}][\tilde{M}], \quad (2)$$

where the rotation transformation matrix $[a]$ is given by

$$[a] = \begin{pmatrix} \cos\eta & 0 & -\sin\eta \\ 0 & 0 & 1 \\ \sin\eta & 0 & \cos\eta \end{pmatrix}$$

and the bond stress transformation matrix $[M]$ is derived from $[a]$.[5,6]

Therefore, the piezoelectric stress tensor $\bar{e'}$ for propagation at an arbitrary angle η in the XZ plane of a zincblende crystal is given by

$$\bar{e'} = \begin{pmatrix} 0 & 0 & 0 & e'_{x4} & 0 & e'_{x6} \\ e'_{y1} & 0 & e'_{y3} & 0 & e'_{y5} & 0 \\ 0 & 0 & 0 & e'_{z4} & 0 & e'_{z6} \end{pmatrix} \quad (3)$$

with

$$\begin{aligned} e'_{x4} &= e_{x4}\cos 2\eta, \\ e'_{x6} &= -e_{x4}\sin 2\eta, \\ e'_{y1} &= -e_{x4}\sin 2\eta, \\ e'_{y3} &= e_{x4}\sin 2\eta, \\ e'_{y5} &= e_{x4}\cos 2\eta, \\ e'_{z4} &= e_{x4}\sin 2\eta, \\ e'_{z6} &= e_{x4}\cos 2\eta. \end{aligned}$$

In order to cast $\bar{e'}$ into a more suitable form for cylindrical quantum wires, we made a transformation from the Cartesian coordinate system to the cylindrical coordinate system. In the cylindrical polar coordinate system, the piezoelectric stress tensor $\bar{e'}$ for propagation at an angle η in the XZ plane of a zincblende crystal transforms as

$$\bar{e''} = [a'][\bar{e'}][\tilde{M}], \quad (4)$$

where the coordinate transformation matrix $[a']$ is given by

[a]Electronic mail: bananisen@ieee.org.
[b]Also at: Physics Department, University of Illinois at Chicago, Chicago, IL 60607, USA; Bioengineering Department, University of Illinois at Chicago, Chicago, IL 60607, USA.
[c]Also at: Physics Department, University of Illinois at Chicago, Chicago, IL 60607, USA.

JOURNAL OF APPLIED PHYSICS **110**, 024506 (2011)

Piezoelectricity in wurtzite polar semiconductor nanowires: A theoretical study

Banani Sen,[a] Michael Stroscio,[b] and Mitra Dutta[c]
Department of Electrical and Computer Engineering, University of Illinois at Chicago, Chicago, Illinois 60607, USA

(Received 28 April 2011; accepted 22 May 2011; published online 22 July 2011)

By considering acoustic phonon mode displacements in nanowires, the piezoelectrically induced electric polarization vector and the associated potential are calculated. For the case of charge-free semiconductor nanowires, the piezo energies generated by strains applied in different directions are compared. For the directions considered, it is found that the maximum piezo energy in these nanowires is generated for strain applied in the vertical direction (i.e., along z-axis). Moreover, for these nanowires, energy generation in AlN and ZnO are found to be superior to GaN, just as expected based on past treatments of nanowires using phonons of bulk structures. © *2011 American Institute of Physics*. [doi:10.1063/1.3603036]

I. INTRODUCTION

Energy harvesting has been around for centuries in the form of windmills, watermills, and passive solar power systems. Among the different forms of energy harvesting, vibration-based mechanical energy being the most ubiquitous and accessible energy source in the surroundings, harvesting this type of energy exhibits a great potential for remote or wireless sensing, charging batteries, and powering electronic devices. Over the last decade, much research has been focused on energy harvesting using piezoelectric semiconductor nanowires to harvest energy on the microscale and nanoscale.[1,2] Owing to the small size and high flexibility of the nanowires, the nanogenerators are very sensitive to small level mechanical disturbances and are ideal for powering wireless sensors, microrobots, nano/micro electro-mechanical systems (NEMS/MEMS) and bioimplantable devices.[3,4] Yet, the physics behind the electromechanical phenomena of these semiconductors is poorly studied. In this paper we have presented a detailed study of the electromechanical phenomena in light of the piezoelectric polarization of these materials.

The piezoelectric interaction occurs in all polar crystals lacking an inversion symmetry. On application of an external strain to a piezoelectric crystal, a macroscopic polarization is produced as a result of the displacements of ions. Thus, an acoustic phonon mode will drive a macroscopic polarization in a piezoelectric crystal. The polar crystals are generally of three types: the wurtzite, the zincblende and the rock salt. The wurtzites are the most stable and therefore most commonly considered at ambient conditions. The zinc blende form can be stabilized using substrates with cubic lattice structure and the rarely found rocksalt (NaCl-type) structure is only observed at relatively high pressures. In this paper we have restricted ourselves to the most common type, i.e., the hexagonal wurtzite structure.

[a]Electronic mail: bananisen@ieee.org.
[b]Also at Physics Department, University of Illinois at Chicago, Chicago, Illinois 60607, USA and Bioengineering Department, University of Illinois at Chicago, Illinois 60607, USA.
[c]Also at Physics Department, University of Illinois at Chicago, Chicago, Illinois 60607, USA.

II. THEORY

In order to determine the piezoelectric polarization in a wurtzite material, it is necessary to consider the piezoelectric tensor of the material under consideration and to determine the strain components corresponding to the deformation under consideration. The piezoelectric tensor relating the piezoelectric polarization vector and the acoustic strain vector may be expressed in matrix notation for the case of a wurtzite crystal in Cartesian coordinates as

$$\bar{e} = \begin{pmatrix} 0 & 0 & 0 & 0 & e_{x5} & 0 \\ 0 & 0 & 0 & e_{x5} & 0 & 0 \\ e_{z1} & e_{z1} & e_{z3} & 0 & 0 & 0 \end{pmatrix}. \tag{1}$$

For the case of uniform plane wave propagation at an arbitrary angle η in the XZ plane of a wurtzite crystal, the piezoelectric stress matrix transforms as

$$\overline{e'} = [a]\,[\bar{e}]\,[\tilde{M}], \tag{2}$$

where the rotation transformation matrix [a] is given by

$$[a] = \begin{pmatrix} \cos\eta & 0 & -\sin\eta \\ 0 & 0 & 1 \\ \sin\eta & 0 & \cos\eta \end{pmatrix}$$

and the bond stress transformation matrix [M] is derived from [a].[5]

Therefore, the piezoelectric stress tensor $\overline{e'}$ for propagation at an arbitrary angle η in the XZ plane of a wurtzite crystal is given by

$$\overline{e'} = \begin{pmatrix} e'_{x1} & e'_{x2} & e'_{x3} & 0 & e'_{x5} & 0 \\ 0 & 0 & 0 & e'_{y4} & 0 & e'_{y6} \\ e'_{z1} & e'_{z2} & e'_{z3} & 0 & e'_{z5} & 0 \end{pmatrix} \tag{3}$$

with

$$e'_{x1} = -e_{z1}\sin\eta\cos^2\eta - e_{z3}\sin^3\eta - e_{x5}\cos\eta\sin 2\eta,$$
$$e'_{x2} = -e_{z1}\sin\eta,$$
$$e'_{x3} = -e_{z1}\sin^3\eta - e_{z3}\cos^2\eta\sin\eta + e_{x5}\cos\eta\sin 2\eta[?],$$
$$e'_{x5} = -e_{z1}\frac{\sin\eta\sin 2\eta}{2} + e_{z3}\frac{\sin\eta\sin 2\eta}{2} + e_{x5}\cos\eta\cos 2\eta,$$

JOURNAL OF APPLIED PHYSICS **112**, 024517 (2012)

Piezoelectricity in lead zirconate titanate nanowires: A theoretical study

Banani Sen,[a] Michael Stroscio,[b] and Mitra Dutta[c]
Department of Electrical and Computer Engineering, University of Illinois at Chicago, Illinois 60607, USA

(Received 17 May 2012; accepted 9 June 2012; published online 25 July 2012)

The piezoelectric coefficients for lead zirconate titanate (PZT) being an order of magnitude higher than the piezoelectric semiconductors, it is expected that this piezoceramic would be very promising for mechanical energy harvesting. This paper presents a systematic evaluation of the piezoelectric potential generated in charge-free PZT nanowires upon application of mechanical strain in different directions. Similar to wurtzite semiconductor nanowires, in case of PZT wires of rocksalt crystal structure, it is found that the stretching modes generate higher potential than the bending mode. However, in spite of high piezoelectric coefficients, the piezoelectric potential generated from these piezoceramic wires is much lower than the semiconductor nanowires because of their high dielectric constant. © *2012 American Institute of Physics*. [http://dx.doi.org/10.1063/1.4737257]

I. INTRODUCTION

The decreasing power requirements for nanodevices open the frontier of energy harvesting from otherwise wasted energy from the environment. An intriguing possibility is the utilization of work produced by the human body via daily activities. Piezoelectric materials have attracted much interest of researchers dealing with recent areas for electromechanical energy conversion technologies. Lead zirconate titanate $Pb[Zr_xTi_{1-x}]O_3$; $0 \le x \le 1$, a ceramic perovskite material is considered as a promising piezoelectric material because of its relatively high piezoelectric coefficients.[1–4] In this paper, we have presented a detailed study of the electromechanical phenomena in PZT in light of the piezoelectric polarization of these materials.

II. THEORY

Direct piezoelectricity may be defined as the electric polarization produced by mechanical strain in certain classes of crystals. The piezoelectric polarization is proportional to the strain and changes sign with it.[5] In mathematical notation, piezoelectrically induced electric polarization vector $\overline{P}$ is given as

$$\overline{P} = \overline{e} \cdot \overline{S}, \tag{1}$$

where $\overline{e}$ is the piezoelectric stress tensor and $\overline{S}$ is the acoustic strain vector.

The piezoelectric stress tensor for a tetragonal crystal system in matrix notation may be expressed as

$$\overline{e} = \begin{pmatrix} 0 & 0 & 0 & 0 & e_{x5} & 0 \\ 0 & 0 & 0 & e_{x5} & 0 & 0 \\ e_{z1} & e_{z1} & e_{z3} & 0 & 0 & 0 \end{pmatrix}. \tag{2}$$

To cast $\overline{e}$ into a form suitable for cylindrical quantum wires, it is necessary to express $\overline{e}$ in a more general form where the co-ordinate axes are rotated with respect to the principal axes of the crystal. Upon applying the rotation transformation matrices of Auld,[6] the piezoelectric stress tensor for phonon propagation at an arbitary angle η in the XZ plane of a tetragonal crystal in cylindrical polar co-ordinate system [r, ϕ, z] transforms as

$$\overline{e''} = [a'][\overline{e'}][\tilde{M}'], \tag{3a}$$

with

$$\overline{e'} = [a][\overline{e}][\tilde{M}], \tag{3b}$$

where the rotation transformation matrix $[a]$ and $[a']$ are given as

$$[a] = \begin{pmatrix} \cos\eta & 0 & -\sin\eta \\ 0 & 0 & 1 \\ \sin\eta & 0 & \cos\eta \end{pmatrix}, \quad [a'] = \begin{pmatrix} \cos\phi & \sin\phi & 0 \\ -\sin\phi & \cos\phi & 0 \\ 0 & 0 & 1 \end{pmatrix},$$

and the bond stress transformation matrices $[M]$ and $[M']$ are derived from $[a]$ and $[a']$, respectively.[7–9]

Therefore, the piezoelectrically induced electric polarization vector $\overline{P}$ in cylindrical polar co-ordinates in terms of the piezoelectric tensor $\overline{e''}$ and the acoustic strain vector $\overline{S}$ may be written as

$$\overline{P} = \overline{e''} \cdot \overline{S}, \tag{4}$$

where $\overline{P}$ is a three component vector and $\overline{S}$ is the six-component strain vector. The six strain components in cylindrical polar co-ordinate system with v being the velocity associated with the acoustic phonon displacement u and ω being the harmonic frequency assumed for the phonon field, i.e., $v = i\omega u$ are[7–9]

[a]Electronic mail: bananisen@ieee.org.
[b]Also at Physics Department and Bioengineering Department, University of Illinois at Chicago, Illinois 60607, USA.
[c]Also at Physics Department, University of Illinois at Chicago, Illinois 60607, USA.

Section VI: Phonon Engineering in Nanostructures --- Optoelectronic Devices and MOSFETs

JOURNAL OF APPLIED PHYSICS 114, 054312 (2013)

Interface optical phonon modes in wurtzite quantum heterostructures

Nanzhu Zhang,[1] Sicheng Liao,[1,2] Mitra Dutta,[1,2] and Michael A. Stroscio[1,2,3,a)]
[1]*Department of Electrical and Computer Engineering, University of Illinois at Chicago, Chicago, Illinois 60607, USA*
[2]*Department of Physics, University of Illinois at Chicago, Chicago, Illinois 60607, USA*
[3]*Department of Bioengineering, University of Illinois at Chicago, Chicago, Illinois 60607, USA*

(Received 30 May 2013; accepted 22 July 2013; published online 6 August 2013)

Simple analytical expressions are derived, herein, for the interface phonon modes of complex SiC- and GaN-based substrates. These analytical results are essential for studies of remote polar-optical phonon phenomena in a variety of structures including heterostructures, in two-dimensional (2D) structures such and graphene, BN, and MoS_2 on polar substrates, as well as in efforts to control the bandgaps of such 2D structures through interactions with polar substrates. © *2013 AIP Publishing LLC*. [http://dx.doi.org/10.1063/1.4817528]

I. INTRODUCTION

Wide band-gap nitride materials has potential applications in UV lasing and sensing[1,2] and high-power devices that are able to work in extreme environments.[3–7] So, they have attracted interest in recent years. These group III materials belong to the hexagonal wurtzite crystal structure that has lower symmetry compared to their zinc-blende counterparts. Therefore, there exist more phonon branches in wurtzite materials (nine optical and three acoustic modes).[8,9] These phonon modes have distinct dynamics and interaction with carriers.

As is well-known, optical phonons make a dominant contribution to scattering processes in polar semiconductor quantum heterostructures. In these structures, they govern a number of processes including hot-electron relaxation, electron interband transition, room temperature exciton recombination, and transport properties.[10–16] Past theoretical investigations have been performed on the interface optical-phonon modes for cubic and wurtzite structures.[17–23] However, many of these investigations were performed on the wurtzite cylindrical quantum wires,[24–27] symmetric structures[28] or periodic superlattice structures.[29,30] For asymmetric wurtzite structures, the phonon dispersion relation is much more complicated due to its optical anisotropy.[31,32] A lot of work has been done on the one interface wurtzite quantum heterostructure case.[33,34] Here we derive the dispersion relation and phonon potential for a two-interface wurtzite quantum heterostructures (Fig. 1) using Loudon's uniaxial and macroscopic dielectric continuum model.[35]

The paper is organized as follows. In Sec. II, we give the analytical solutions of the dispersion relation of interface optical phonon modes and electrostatic potentials in the structure. These solutions are applied to special cases of SiC/GaN/vacuum and GaN/AlN/Vacuum heterostructures and the results and discussions are given in Sec. III. We summarize the paper and conclude in Sec. IV.

II. THEORY

Wurtzite crystal structure has a c axis that is perpendicular to the hexagonal planes. We take the c axis along the z direction, which is perpendicular to the heterointerfaces, and denote the direction perpendicular to c axis as ⊥. Due to the optical anisotropy of wurtzite structure, the long wavelength optical phonon modes can be divided into two groups, ordinary and extraordinary phonons, based on the mutual orientation between the c axis, the phonon wave vector q, the electric field E, and the polarization field P. Following Loudon's theory for uniaxial crystals, only one group of three optical phonon branches is infrared active. At the Γ point in the Brillion zone of wurtzite crystal, only the z-polarized phonon with A_1 symmetry and ⊥-polarized phonon with E_1 symmetry are infrared active among the nine optical-phonon modes. Within the macroscopic dielectric continuum model, the field associated with the optical phonon modes in the non-retardation limit satisfies the classical electrostatic equations[36]

$$E(r) = -\nabla\Phi(r), \tag{1}$$

$$D(r) = E(r) + 4\pi P(r) = \varepsilon_{\perp}(\omega)E_{\perp}(r)\hat{\rho} + \varepsilon_z(\omega)E_z(r)\hat{z}, \tag{2}$$

$$\nabla D(r) = 0, \tag{3}$$

where E is the electric field, D is the displacement, P is the polarization field, and Φ is the electrostatic potential due to the optical phonon mode. z and ρ denote the unit vector parallel and perpendicular to z direction, respectively. We assumed that there is no charge transfer between ions. $\varepsilon_{\perp}$ and ε_z are the frequency-dependent dielectric functions parallel and perpendicular to z directions. They are given as[37,38]

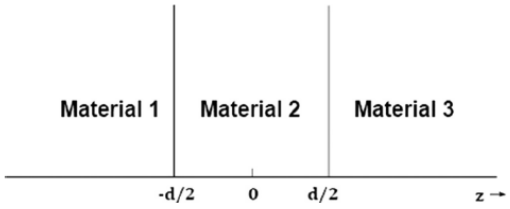

FIG. 1. Schematic diagram showing a two-interface heterostructure composed of three arbitrary wurtzite materials.

a)stroscio@uic.edu

Solid-State Electronics 94 (2014) 72–81

Contents lists available at ScienceDirect

Solid-State Electronics

journal homepage: www.elsevier.com/locate/sse

Interface phonon modes of dual-gate MOSFET system

Nanzhu Zhang [a,*], Mitra Dutta [a,b], Michael A. Stroscio [a,b,c]

[a] Electrical and Computer Engineering, University of Illinois at Chicago, Chicago, IL 60607, United States
[b] Departments of Physics, University of Illinois at Chicago, Chicago, IL 60607, United States
[c] Bioengineering, University of Illinois at Chicago, Chicago, IL 60607, United States

ARTICLE INFO

Article history:
Received 25 September 2013
Received in revised form 12 December 2013
Accepted 30 January 2014
Available online 15 March 2014

The review of this paper was arranged by Prof. E. Calleja

Keywords:
High-k dielectrics
Dual-gate MOSFET
Interface phonon modes

ABSTRACT

Herein, analytical expressions are derived for the interface phonon modes of the dual-gate MOSFET system. These analytical results are essential for studies of phonon scattering in MOSFET structures which will affect the performance of the device. We consider selected cubic systems within the framework of macroscopic dielectric continuum model. A principal finding of this paper is that the normally-dominant and unwanted carrier scattering caused by interface phonon interactions can be strongly suppressed through the appropriate placement of the two gates.

1. Introduction

In recent years, considerable research has been devoted to means of increasing the gate capacitance so as to increase the drive current of a MOSFET (metal–oxide-semiconductor field-effect transistor). As is well known, silicon dioxide (SiO_2) is a widely used insulator separating the gate and the semiconductor. However, due to leakage current increases the thickness of SiO_2 cannot be decreased below the 1.5–1.0 nm range which is required by device scaling. This drawback of SiO_2 has motivated efforts to find new materials to replace it. Recently, a considerable amount of effort has been devoted to high-k dielectrics whose dielectrics constant k is larger than that of SiO_2 in order to increase the overall capacitance and then increase the drive current. However, there is still a problem that needs to be solved if SiO_2 is replaced with a high-k dielectric. A high-k dielectric is a material with a high dielectric constant k which results from both the ionic and the electronic polarization. For an insulator, a higher dielectric constant can only come from a large ionic polarization because the bandgap of the insulator is too large to increase the electronic polarization. We know that large ionic response dominates at low frequency which result in a large static dielectric constant while large static dielectric constant lead to large scattering strength because it is proportional to $\hbar\omega_{to}\left[\frac{1}{\varepsilon^{\infty}}-\frac{1}{\varepsilon^{0}}\right]$. As a result of the large scattering strength associated with low frequencies, the effective electron mobility in the inversion layer of the MOS system is reduced [1]. It is this disadvantage of high-k dielectrics that prompts us to consider using a dual-gate structure to avoid the scattering caused by the phonon modes existing in the system.

The principal goal of this paper is to show that all of the interface phonon modes – which are generally dominant in the electron–phonon scattering processes – make considerably reduced contributions when metallic boundaries are selected appropriately. This is of particular importance in nanoscale structures where the interface phonon modes generally dominant in the scattering of carrier from phonon modes. Indeed, in Ref. [2], it is demonstrated that establishing metal–semiconductor interfaces at the heterojunctions of semiconductor quantum wells with the semiconductor–metal boundary conditions dramatically reduces or eliminates unwanted carrier energy loss caused by interactions with interface longitudinal-optical (LO) phonon modes. Moreover, in Ref. [3], study of the Hamiltonian describing the interaction of both confined longitudinal-optical and surface-optical photons with charge carriers, demonstrates that the interaction by the surface-optical phonon modes is very strong and may dominate over other scattering processes, especially with dimensions of about 100 A or less. Ref. [6] provides additional examples of the dominance of carrier–interface-phonon scattering among the phonon scattering mechanisms. Because of the typically dominant role of the interface phonon modes among the phonon scattering processes in nanostructures, and because of the frequent dominance of phonon scattering processes in nanodevices, it is important to

* Corresponding author. Tel.: +1 3123408868.
E-mail addresses: nzhang7@uic.edu (N. Zhang), stroscio@uic.edu (M.A. Stroscio).

http://dx.doi.org/10.1016/j.sse.2014.01.007
0038-1101/

Section VII: PAPERS PUBLISHED OR IN PRESS

Sidra Farid, Souvik Mukherjee, Hye-Son Jung, Michael Stroscio, and Mitra Dutta, Analysis on the structural, vibrational and defect states of chlorine treated polycrystalline cadmium telluride structures grown by e-beam evaporation, Mater. Res. Express, 2, 025007 (2015).

N. Zhang, M. Dutta and M. A. Stroscio, Interface Phonon Modes of Dual-Gate MOSFET System, Solid State Electronics, 94, 72-81 (2014).

Shripriya Poduri, Michael A. Stroscio, and Mitra Dutta, Characterization of CdS nanowires self assembled in a nanoporous alumina template, Journal of Electronic Materials, 43(11), 3979-3983 (2014).

Yi Lan, Nanzhu Zhang, J. (Lucy) Shi, M. Dutta, M. A. Stroscio, "Enhanced signal-to-noise in photodetectors due to interface phonon-assisted transitions, 2014 International Workshop on Computational Electronics (IWCE), Paris, INSPEC Accession Number: 14485107, August 2014

Sidra Farid, Souvik Mukherjee, Hye-Son Jung, Michael Stroscio, and Mitra Dutta, Analysis on the structural, vibrational and defect states of chlorine treated polycrystalline cadmium telluride based nanostructures" submitted to Nanotechnology, October 2014; NANO-105273

N. Zhang, M. A. Stroscio and M. Dutta, Interface Phonon Modes of Dual-Gate MOSFET System, Proceedings of the International Workshop on Computational Electronics, Nara, Japan, Society of Micro- and Nanoelectronics, 216-217 (2013); ISBN 978-3-901578-26-7

N. Zhang, M. A. Stroscio and M. Dutta, Interface Phonon Modes of Dual-Gate MOSFET System, Proceedings of the International Workshop on Computational Electronics, Nara, Japan, Society of Micro- and Nanoelectronics, 216-217 (2013); ISBN 978-3-901578-26-7

M. S. Choi, M. A. Stroscio, and M. Dutta, Effect of the Size and the Separation of Metal Nanodots on the Electromagnetic Enhancement to Surface-enhanced Raman Spectroscopy, Proceedings of the International Workshop on Computational Electronics, Nara, Japan, Society of Micro- and Nanoelectronics, 198-199 (2013); ISBN 978-3-901578-26-7

N. Zhang, Sicheng Laio, M. Dutta and M. A. Stroscio, Interface Optical Phonon Modes in Wurtzite Quantum Heterostructures, Journal of Applied Physics, 114, 054312 (2013).

Mohsen Purahmad, Michael A. Stroscio, and Mitra Dutta, A theoretical study on the effect of piezoelectric charges on the surface potential and surface depletion region of ZnO nanowires, Journal of Semiconductor Science and Technology, 28(1), 015019 (2013).

M. Purahmad, M. A. Stroscio and M. Dutta, Modeling the Effect of Nanowire Size on the Piezoelectric Nanogenerators Output, Proceedings of the International Workshop on Computational Electronics, Nara, Japan, Society of Micro- and Nanoelectronics, 240-241 (2013); ISBN 978-3-901578-26-7

N. Zhang, M. A. Stroscio and M. Dutta, Interface Phonon Modes of Dual-Gate MOSFET System, Proceedings of the International Workshop on Computational Electronics, Nara, Japan, Society of Micro- and Nanoelectronics, 216-217 (2013); ISBN 978-3-901578-26-7

M. S. Choi, M. A. Stroscio, and M. Dutta, Effect of the Size and the Separation of Metal Nanodots on the Electromagnetic Enhancement to Surface-enhanced Raman Spectroscopy, Proceedings of the International Workshop on Computational Electronics, Nara, Japan, Society of Micro- and Nanoelectronics, 198-199 (2013); ISBN 978-3-901578-26-7

Jun Qian, Mitra Dutta, and Michael A. Stroscio, Phonon bottleneck effects in rectangular graphene quantum dots, Journal of Computational Electronics, 11(3) 293-301 (2012).

S. Farid, M. Purahmad M. A. Stroscio, and M. Dutta, Computational analysis of the emission of ZnO nanowires and coreshell CdSe/ZnS quantum dots deposited on different substrates, IEEE Proceedings of the International Workshop on Computational Electronics, pages 207-208, 2012.

Biswas S., Gosztola D. J., Wiederrecht G. P., Stroscio M. A. and Dutta M., "Annealing-Induced Morphological Changes in Nanocrystalline Quantum Dots and Their Impact on Charge Transport Properties", J. Electro. Mater., 41, 524-529, (2012).

Biswas S., Jung H., Stroscio M. A. and Dutta M." Morphology, Optical Properties, Charge Transfer, and Charge Transport in Nanocrystalline Quantum Dots", Proc. SPIE: Quantum Dots and Nanostructures: Synthesis, Characterization, and Modeling IX, 827108, (2012).

N. Zhang, Sicheng Laio, M. Dutta and M. A. Stroscio, Interface Optical Phonon Modes in Wurtzite Quantum Heterostructures, Journal of Applied Physics, 114, 054312 (2013) on line August 6, 2013.

Zhiping Wang, Kitt Reinhardt, Mitra Dutta, Michael A. Stroscio, Phonons in bulk and low-dimensional systems, in the book on Phonons, Edited by Gyaneshwar Srivastava and Subhash Shinde, in press, Springer Publishing Co., 2011.

Banani Sen, M. Dutta, and M. Stroscio, Photoluminescence and Raman Spectroscopy of Polycrystalline ZnO Nanofibers Deposited by Electrospinning, Journal of Electronic Materials, published on-line Journal of Electronic Materials, DOI: 10.1007/s11664-011-1688-8, Springer (2011).

Banani Sen, Michael Stroscio, and Mitra Dutta, Piezoelectricity in Wurtzite Polar Semiconductor Nanowires: A Theoretical Study, Journal of Applied Physics, 110, 024506 (2011).

Ayan Kar, Michael Stroscio, Mitra Dutta, and Meyya Meyyappan, Electronic Properties of Y-junctions in SnO2 Nanowires, Phys. Status Solidi B, 1–5 (2011) / DOI 10.1002/pssb.201147233

Ayan Kar, Michael A. Stroscio, M. Meyyappan, David J. Gosztola, Gary P. Weiderrecht, Mitra Dutta, Tailoring the Surface Properties and Carrier Dynamics in SnO2 Nanowires, Nanotechnology, 22, 285709-1-7 (2011).

Sushmita Biswas, Yang Li, Michael A. Stroscio, and Mitra Dutta, Charge Transport in Two Conductive Polymer and Semiconducting Quantum Dot Nanocomposite Systems, Journal of Applied Physics, 111, 044313-1-16 (2012).

Banani Sen, Michael Stroscio, and Mitra Dutta, Piezoelectricity in Zinc Blende Polar Semiconductor Nanowires: A Theoretical Study, Journal of Applied Physics, 111, 054514 (2012).

Banani Sen, Michael Stroscio, and Mitra Dutta, Piezoelectricity in Lead Zirconate Titanate Semiconductor Nanowires: A Theoretical Study, Journal of Applied Physics, 112, 024517-1-6 (2012).

Ayan Kar, Ryan Ahern, N. Gopalsami, A. C. Raptis, Michael A. Stroscio, and Mitra , Preliminary investigation on the modification of electronic properties in surface passivated SnO2 nanowires with Schottky contacts on being exposed to 137Cs gamma-radiation, Journal of Applied Physics, 111, 084319 (2012).

Zhiping Wang, Nanzhu Zhang, Kimber Brenneman, Tsai Chin Wu, Hyeson Jung, Sushmita Biswas, Banani Sen, Kitt Reinhardt, Sicheng Liao, Michael A. Stroscio, and Mitra Dutta, Optoelectronic Applications of Colloidal Quantum Dots, in Chapter 15 of Quantum Dot Devices, pages 351-367, Edited by Zhiming M. Wang, Springer Publishing Co., 2012; this book is Vol. 13 of Lecture Notes in Nanoscale Science and Technology, ISBN 978-1-4614-3569-3

Section VIII: PRESENTATIONS

Yi Lan, Nanzhu Zhang, Lucy Shi, Chenjie Tang, Mitra Dutta and Michael A. Stroscio, Design of a Novel Heterostructure Photodetectors with Dramatically Enhance Signal-to-Noise based on Resonant Interface-Phonon-Assisted Transitions and Engineering of Energy States to Enhance Transition Rates, Optics-2014, 2nd International Conference and Exhibition on Lasers, Optics & Photonics, September 10, 2014 Philadelphia, USA (2014) (Invited)

Mitra Dutta, Ayan Kar, Mohsen Purahmad, Sidra Farid, Mojgan Mazouchi, Xenia Meshik, Michael A. Stroscio et al, Growth and characterization studies of oxide nanowires: Tin Oxide, Zinc Oxide and Indium Oxide, Optics-2014, 2nd International Conference and Exhibition on Lasers, Optics & Photonics, September 9, 2014 Philadelphia, USA (2014) (Invited)

Yi Lan, Chenjie Tang, Nanzhu Zhang, Lucy Shi, Mitra Dutta and Michael A. Stroscio, Resonant Interface-Phonon-Assisted Transitions to Enhance Transition Rates in Single-Well--Double-Well Heterostructure Photodetectors, submitted to PHONONS 2015

Shripriya Poduri, Mitra Dutta, and Michael A. Stroscio, Study of Anisotropy of electron-phonon coupling for grown CdS nanowires, submitted to PHONONS 2015

Min S. Choi, Mitra Dutta, and Michael A. Stroscio, Numerical Analysis of Scattering Cross Section of Non-Precious Metallic Plasmonic Nanodisks, submitted to International Workshop on Computational Electronics, IWCE 2015.

Shripriya Poduri, Mitra Dutta, and Michael A. Stroscio, Study of Polarization Anisotropy of grown Cadmium sulphide nanowires, submitted to Argonne National Laboratory Center for Nanoscale Technology, 2015.

Yi Lan, Chenjie Tang, Junxia (Lucy) Shi, Mitra Dutta, Michael Stroscio, Phononic Properties for Enhanced Signal-to-Noise Photodetector, submitted to International Workshop on Computational Electronics, IWCE 2015.

C. Huang, S. Poduri, M.A. Stroscio, and M. Dutta, Simulation of Current-Voltage Curves for CdS Cylinders Embedded in P3HT, submitted to International Workshop on Computational Electronics, IWCE 2015.

Sidra Farid, MichAEL Stroscio, and Mitra Dutta, Modeling CdS/CdTe interface properties for improving solar cell photoelectric quantum yield, AAAS Meeting, Chicago, February 2014.

Shripriya Poduri, Michael Stroscio, and Mitra Dutta, Photoluminescence characterization of Cadmium Sulphide (CdS) nanowires for polarization studies, AAAS Meeting, Chicago, February 2014.

Li Yan, Nanzhu Zhang, Junxia (Lucy) Shi, M. Dutta and M. A. Stroscio, Enhanced Signal-to-Noise in Photodetectors due to Interface Phonon-assisted Transitions, International Workshop on Computational Electronics, Paris, France, July 2014.

Yi Lan, Nanzhu Zhang, Lucy Shi, Chenjie Tang, Mitra Dutta and Michael A. Stroscio, Design of a Novel Heterostructure Photodetectors with Dramatically Enhance Signal-to-Noise based on Resonant Interface-Phonon-Assisted Transitions and Engineering of Energy States to Enhance Transition Rates, Optics-2014, 2nd International Conference and Exhibition on Lasers, Optics & Photonics, September 10, 2014 Philadelphia, USA (2014) (Invited)

Mitra Dutta, Ayan Kar, Mohsen Purahmad, Sidra Farid, Mojgan Mazouchi, Xenia Meshik, Michael A. Stroscio et al, Growth and characterization studies of oxide nanowires: Tin Oxide, Zinc Oxide and Indium Oxide, Optics-2014, 2nd International Conference and Exhibition on Lasers, Optics & Photonics, September 9, 2014 Philadelphia, USA (2014) (Invited)

M. Purahmad, M. A. Stroscio and M. Dutta, Modeling the Effect of Nanowire Size on the Piezoelectric Nanogenerators Output, International Workshop on Computational Electronics, Nara, Japan, June 2013.

N. Zhang, M. A. Stroscio and M. Dutta, Interface Phonon Modes of Dual-Gate MOSFET System, International Workshop on Computational Electronics, Nara, Japan, June 2013.

M. S. Choi, M. A. Stroscio, and M. Dutta, Effect of the Size and the Separation of Metal Nanodots on the Electromagnetic Enhancement to Surface-enhanced Raman Spectroscopy, International Workshop on Computational Electronics, Nara, Japan, June 2013.

Michael A. Stroscio, Mitra Dutta, Sicheng Liao, Banani Sen, Jun Qian, Robin Xu, Nanzhu Zhang, Min Choi, Yi Lan, Kimber Brenneman, Xenia Meshik, Preeti Pratap, and Donna Wu, Applications of Physics in Nanoscience and Nanoelectronics, Seminar at Ball State University, March 28, 2013.

Michael A. Stroscio and Mitra Dutta, Phonons in Nanostructures, University of New Mexico, May 2012.

Sushmita Biswas, Nanzhu Zhang, M. A. Stroscio, and M. Dutta, Conductive Polymer and Semiconducting Quantum Dots Nanocomposite Systems, International Workshop on Computational Electronics, Madison, Wisconsin, May 2012.

Banani Sen, M. A. Stroscio, and M. Dutta, Piezoelectric Fields in Quantum Wires, International Workshop on Computational Electronics, Madison, Wisconsin, May 2012.

M. Purahmad, S. Farid, M. A. Stroscio and M. Dutta, Influence of Piezoelectric Charges on the Surface Depletion Thickness of ZnO Nanowires, International Workshop on Computational Electronics, Madison, Wisconsin, May 2012.

M. Purahmad, S. Farid, M. A. Stroscio and M. Dutta, Influence of Substrates on the Optical Characteristics of ZnO Nanowires and Coreshell CdSe/ZnS Quantum Dots, International Workshop on Computational Electronics, Madison, Wisconsin, May 2012.

Sidra Farid, Michael A. Stroscio, Mitra Dutta, Raman Scattering Investigations of CdS Thin Films grown by Thermal Evaporation,PHONONS, 2012, July 8-12, 2012, Ann Arbor, Michigan.

Michael A. Stroscio, Mitra Dutta, Banani Sen, Ke Xu, Jun Qian, and Ke Sun, Phonons in Nanostructures, Phonon School, International Workshop on Computational Electronics, University of Wisconsin, June 2012; presentation included on the web report of the Phonon School at http://iwce2012.engr.wisc.edu/ (Invited)

Section IX: Recognition and Service

MAS service includes: throughout this grant served as AF SAB member and as a consultant; NRC Board on Army Science and technology. MAS was appointed UIC Distinguished Professor in 2014, in part, for this AFOSR sponsored research. MD became a Fellow of the APS in 2013, in part, for this AFOSR sponsored research.

1.

1. Report Type

Final Report

Primary Contact E-mail

Contact email if there is a problem with the report.

stroscio@uic.edu

Primary Contact Phone Number

Contact phone number if there is a problem with the report

312-413-5968

Organization / Institution name

University of Illinois at Chicago

Grant/Contract Title

The full title of the funded effort.

MULTI-FUNCTIONAL UV-VISIBLE-IR NANOSENSORS DEVICES AND STRUCTURES

Grant/Contract Number

AFOSR assigned control number. It must begin with "FA9550" or "F49620" or "FA2386".

FA9550-11-1-0271

Principal Investigator Name

The full name of the principal investigator on the grant or contract.

Michael A Stroscio

Program Manager

The AFOSR Program Manager currently assigned to the award

Dr. Kenneth Goretta

Reporting Period Start Date

09/01/2011

Reporting Period End Date

02/28/2015

Abstract

The investigators have undertaken several quantum engineering and phonon engineering efforts underlying the enhancement of the performance of nanostructure-based sensors and electronic-optoelectronic devices. These include: initial designs of novel photodetectors relying on phonon-assisted transitions as well as photon absorption events; the use of colloidal quantum dots as optoelectronic elements; investigating novel nanostructures (including graphene and CNTs as contacts) as components of quantum-dot based optoelectronic devices; investigating confined phonon effects in novel components of the integrated nanostructure-based optoelectronic structures; investigating full-tensor piezoelectric properties of nanostructures including nanowires; and the investigation of photodetector structures from these nanostructures and conducting polymers. This research includes modeling and theory of quantum wires and quantum dots for opto-electronic, piezoelectric, and electronic applications including sensors and piezoelectric components.

This research program addresses systematic theoretical and experimental investigations

of nanostructure-based electronic and optoelectronic structures with the goal of facilitating major improvements in the performance levels of nanodevices beyond the current state-of-the-art. In particular, this program focuses on research thrusts with objectives including: model, design, fabricate, and experimentally characterize robust multi-functional nano-device structures for enhanced charge transport & collection; model, design, fabricate, and experimentally characterize such nanodevices to optimize device structures with quantum-engineering and phonon-assisted transitions in nanostructures. Quantum engineering of nano-structures is emphasized. Related quantum-wire structures – including piezoelectric quantum wires are included.

Results obtained during this period of this effort include: extending a theory band formation in an array of colloidal quantum dots embedded in conductive polymer; design of a novel single-well double-well heterostructure photodetectors with dramatically enhance signal-to-noise based on resonant interface-phonon-assisted transitions; role of interface optical phonon modes in wurtzite quantum heterostructures; and interface phonon modes of dual-gate MOSFETs
Specific results were obtained on the following topics:
Design of a Novel Heterostructure Photodetectors with Dramatically Enhance Signal-to-Noise based on Resonant Interface-Phonon-Assisted Transitions and Engineering of Energy States to Enhance Transition Rates;
Effect of the Size and the Separation of Metal Nanodots on the Electromagnetic Enhancement to Surface-enhanced Raman Spectroscopy;
Interface Optical Phonon Modes in Wurtzite Quantum Heterostructures;
Interface Phonon Modes of Dual-Gate MOSFET Systems.

Phonon bottleneck effects in rectangular graphene quantum dots,
Theoretical study on the effect of piezoelectric charges on the surface potential and surface depletion region of ZnO nanowires
Modeling the effect of nanowire size on the piezoelectric effects
Interface phonon modes in wurtzite heterostructure systems
Effect of the size and the separation of metal nanodots on the electromagnetic enhancement to surface-enhanced Raman spectroscopy
Annealing-induced morphological changes in nanocrystalline quantum dots and their impact on charge transport properties

Photoluminescence and Raman Spectroscopy of Polycrystalline ZnO Nanofibers Deposited by Electrospinning,
Piezoelectricity in Wurtzite Polar Semiconductor Nanowires: A Theoretical Study,
Electronic Properties of Y-junctions in SnO2 Nanowires,
Tailoring the Surface Properties and Carrier Dynamics in SnO2 Nanowires,
Charge Transport in Two Conductive Polymer and Semiconducting Quantum Dot Nanocomposite Systems,
Piezoelectricity in Zinc Blende Polar Semiconductor Nanowires: A Theoretical Study,
Piezoelectricity in Lead Zirconate Titanate Semiconductor Nanowires: A Theoretical Study,
Electronic properties in surface passivated SnO2 nanowires with Schottky contacts
Phonon bottleneck effects in rectangular graphene quantum dots,
Piezoelectricity Fields in Quantum Wires,
Optoelectronic Applications of Colloidal Quantum Dots.

Distribution Statement

This is block 12 on the SF298 form.

Distribution A - Approved for Public Release

Explanation for Distribution Statement

If this is not approved for public release, please provide a short explanation. E.g., contains proprietary information.

SF298 Form

Please attach your SF298 form. A blank SF298 can be found here. Please do not password protect or secure the PDF The maximum file size for an SF298 is 50MB.

AFOSR SF298 26APR15 AFD-070820-035.pdf

Upload the Report Document. File must be a PDF. Please do not password protect or secure the PDF . The maximum file size for the Report Document is 50MB.

AFOSR FINAL REPORT ATTACHMENT APR15.pdf

Upload a Report Document, if any. The maximum file size for the Report Document is 50MB.

Archival Publications (published) during reporting period:

PAPERS PUBLISHED OR IN PRESS

Sidra Farid, Souvik Mukherjee, Hye-Son Jung, Michael Stroscio, and Mitra Dutta, Analysis on the structural, vibrational and defect states of chlorine treated polycrystalline cadmium telluride structures grown by e-beam evaporation, Mater. Res. Express, 2, 025007 (2015).

N. Zhang, M. Dutta and M. A. Stroscio, Interface Phonon Modes of Dual-Gate MOSFET System, Solid State Electronics, 94, 72-81 (2014).

Shripriya Poduri, Michael A. Stroscio, and Mitra Dutta, Characterization of CdS nanowires self assembled in a nanoporous alumina template, Journal of Electronic Materials, 43(11), 3979-3983 (2014).

Yi Lan, Nanzhu Zhang, J. (Lucy) Shi, M. Dutta, M. A. Stroscio, “Enhanced signal-to-noise in photodetectors due to interface phonon-assisted transitions, 2014 International Workshop on Computational Electronics (IWCE), Paris, INSPEC Accession Number: 14485107, August 2014

Sidra Farid, Souvik Mukherjee, Hye-Son Jung, Michael Stroscio, and Mitra Dutta, Analysis on the structural, vibrational and defect states of chlorine treated polycrystalline cadmium telluride based nanostructures" submitted to Nanotechnology, October 2014; NANO-105273

N. Zhang, M. A. Stroscio and M. Dutta, Interface Phonon Modes of Dual-Gate MOSFET System, Proceedings of the International Workshop on Computational Electronics, Nara, Japan, Society of Micro- and Nanoelectronics, 216-217 (2013); ISBN 978-3-901578-26-7

N. Zhang, M. A. Stroscio and M. Dutta, Interface Phonon Modes of Dual-Gate MOSFET System, Proceedings of the International Workshop on Computational Electronics, Nara, Japan, Society of Micro- and Nanoelectronics, 216-217 (2013); ISBN 978-3-901578-26-7

M. S. Choi, M. A. Stroscio, and M. Dutta, Effect of the Size and the Separation of Metal Nanodots on the Electromagnetic Enhancement to Surface-enhanced Raman Spectroscopy, Proceedings of the International Workshop on Computational Electronics, Nara, Japan, Society of Micro- and Nanoelectronics, 198-199 (2013); ISBN 978-3-901578-26-7

N. Zhang, Sicheng Laio, M. Dutta and M. A. Stroscio, Interface Optical Phonon Modes in Wurtzite Quantum Heterostructures, Journal of Applied Physics, 114, 054312 (2013).

Mohsen Purahmad, Michael A. Stroscio, and Mitra Dutta, A theoretical study on the effect of piezoelectric charges on the surface potential and surface depletion region of ZnO nanowires, Journal of Semiconductor Science and Technology, 28(1), 015019 (2013).

M. Purahmad, M. A. Stroscio and M. Dutta, Modeling the Effect of Nanowire Size on the Piezoelectric Nanogenerators Output, Proceedings of the International Workshop on Computational Electronics, Nara, Japan, Society of Micro- and Nanoelectronics, 240-241 (2013); ISBN 978-3-901578-26-7

N. Zhang, M. A. Stroscio and M. Dutta, Interface Phonon Modes of Dual-Gate MOSFET

System, Proceedings of the International Workshop on Computational Electronics, Nara, Japan, Society of Micro- and Nanoelectronics, 216-217 (2013); ISBN 978-3-901578-26-7
M. S. Choi, M. A. Stroscio, and M. Dutta, Effect of the Size and the Separation of Metal Nanodots on the Electromagnetic Enhancement to Surface-enhanced Raman Spectroscopy, Proceedings of the International Workshop on Computational Electronics, Nara, Japan, Society of Micro- and Nanoelectronics, 198-199 (2013); ISBN 978-3-901578-26-7
Jun Qian, Mitra Dutta, and Michael A. Stroscio, Phonon bottleneck effects in rectangular graphene quantum dots, Journal of Computational Electronics, 11(3) 293-301 (2012).
S. Farid, M. Purahmad M. A. Stroscio, and M. Dutta, Computational analysis of the emission of ZnO nanowires and coreshell CdSe/ZnS quantum dots deposited on different substrates, IEEE Proceedings of the International Workshop on Computational Electronics, pages 207-208, 2012.
Biswas S., Gosztola D. J., Wiederrecht G. P., Stroscio M. A. and Dutta M., "Annealing-Induced Morphological Changes in Nanocrystalline Quantum Dots and Their Impact on Charge Transport Properties", J. Electro. Mater., 41, 524-529, (2012).
Biswas S., Jung H., Stroscio M. A. and Dutta M." Morphology, Optical Properties, Charge Transfer, and Charge Transport in Nanocrystalline Quantum Dots", Proc. SPIE: Quantum Dots and Nanostructures: Synthesis, Characterization, and Modeling IX, 827108, (2012).
N. Zhang, Sicheng Laio, M. Dutta and M. A. Stroscio, Interface Optical Phonon Modes in Wurtzite Quantum Heterostructures, Journal of Applied Physics, 114, 054312 (2013) on line August 6, 2013.
Zhiping Wang, Kitt Reinhardt, Mitra Dutta, Michael A. Stroscio, Phonons in bulk and low-dimensional systems, in the book on Phonons, Edited by Gyaneshwar Srivastava and Subhash Shinde, in press, Springer Publishing Co., 2011.
Banani Sen, M. Dutta, and M. Stroscio, Photoluminescence and Raman Spectroscopy of Polycrystalline ZnO Nanofibers Deposited by Electrospinning, Journal of Electronic Materials, published on-line Journal of Electronic Materials, DOI: 10.1007/s11664-011-1688-8, Springer (2011).
Banani Sen, Michael Stroscio, and Mitra Dutta, Piezoelectricity in Wurtzite Polar Semiconductor Nanowires: A Theoretical Study, Journal of Applied Physics, 110, 024506 (2011).
Ayan Kar, Michael Stroscio, Mitra Dutta, and Meyya Meyyappan, Electronic Properties of Y-junctions in SnO2 Nanowires, Phys. Status Solidi B, 1–5 (2011) / DOI 10.1002/pssb.201147233
Ayan Kar, Michael A. Stroscio, M. Meyyappan, David J. Gosztola, Gary P. Weiderrecht, Mitra Dutta, Tailoring the Surface Properties and Carrier Dynamics in SnO2 Nanowires, Nanotechnology, 22, 285709-1-7 (2011).
Sushmita Biswas, Yang Li, Michael A. Stroscio, and Mitra Dutta, Charge Transport in Two Conductive Polymer and Semiconducting Quantum Dot Nanocomposite Systems, Journal of Applied Physics, 111, 044313-1-16 (2012).
Banani Sen, Michael Stroscio, and Mitra Dutta, Piezoelectricity in Zinc Blende Polar Semiconductor Nanowires: A Theoretical Study, Journal of Applied Physics, 111, 054514 (2012).
Banani Sen, Michael Stroscio, and Mitra Dutta, Piezoelectricity in Lead Zirconate Titanate Semiconductor Nanowires: A Theoretical Study, Journal of Applied Physics, 112, 024517-1-6 (2012).
Ayan Kar, Ryan Ahern, N. Gopalsami, A. C. Raptis, Michael A. Stroscio, and Mitra , Preliminary investigation on the modification of electronic properties in surface passivated SnO2 nanowires with Schottky contacts on being exposed to 137Cs gamma-radiation, Journal of Applied Physics, 111, 084319 (2012).
Zhiping Wang, Nanzhu Zhang, Kimber Brenneman, Tsai Chin Wu, Hyeson Jung, Sushmita Biswas, Banani Sen, Kitt Reinhardt, Sicheng Liao, Michael A. Stroscio, and

Mitra Dutta, Optoelectronic Applications of Colloidal Quantum Dots, in Chapter 15 of Quantum Dot Devices, pages 351-367, Edited by Zhiming M. Wang, Springer Publishing Co., 2012; this book is Vol. 13 of Lecture Notes in Nanoscale Science and Technology, ISBN 978-1-4614-3569-3

Section VIII: PRESENTATIONS

Yi Lan, Nanzhu Zhang, Lucy Shi, Chenjie Tang, Mitra Dutta and Michael A. Stroscio, Design of a Novel Heterostructure Photodetectors with Dramatically Enhance Signal-to-Noise based on Resonant Interface-Phonon-Assisted Transitions and Engineering of Energy States to Enhance Transition Rates, Optics-2014, 2nd International Conference and Exhibition on Lasers, Optics & Photonics, September 10, 2014 Philadelphia, USA (2014) (Invited)

Mitra Dutta, Ayan Kar, Mohsen Purahmad, Sidra Farid, Mojgan Mazouchi, Xenia Meshik, Michael A. Stroscio et al, Growth and characterization studies of oxide nanowires: Tin Oxide, Zinc Oxide and Indium Oxide, Optics-2014, 2nd International Conference and Exhibition on Lasers, Optics & Photonics, September 9, 2014 Philadelphia, USA (2014) (Invited)

Yi Lan, Chenjie Tang, Nanzhu Zhang, Lucy Shi, Mitra Dutta and Michael A. Stroscio, Resonant Interface-Phonon-Assisted Transitions to Enhance Transition Rates in Single-Well--Double-Well Heterostructure Photodetectors, submitted to PHONONS 2015

Shripriya Poduri, Mitra Dutta, and Michael A. Stroscio, Study of Anisotropy of electron-phonon coupling for grown CdS nanowires, submitted to PHONONS 2015

Min S. Choi, Mitra Dutta, and Michael A. Stroscio, Numerical Analysis of Scattering Cross Section of Non-Precious Metallic Plasmonic Nanodisks, submitted to International Workshop on Computational Electronics, IWCE 2015.

Shripriya Poduri, Mitra Dutta, and Michael A. Stroscio, Study of Polarization Anisotropy of grown Cadmium sulphide nanowires, submitted to Argonne National Laboratory Center for Nanoscale Technology, 2015.

Yi Lan, Chenjie Tang, Junxia (Lucy) Shi, Mitra Dutta, Michael Stroscio, Phononic Properties for Enhanced Signal-to-Noise Photodetector, submitted to International Workshop on Computational Electronics, IWCE 2015.

C. Huang, S. Poduri, M.A. Stroscio, and M. Dutta, Simulation of Current-Voltage Curves for CdS Cylinders Embedded in P3HT, submitted to International Workshop on Computational Electronics, IWCE 2015.

Sidra Farid, MichAEL Stroscio, and Mitra Dutta, Modeling CdS/CdTe interface properties for improving solar cell photoelectric quantum yield, AAAS Meeting, Chicago, February 2014.

Shripriya Poduri, Michael Stroscio, and Mitra Dutta, Photoluminescence characterization of Cadmium Sulphide (CdS) nanowires for polarization studies, AAAS Meeting, Chicago, February 2014.

Li Yan, Nanzhu Zhang, Junxia (Lucy) Shi, M. Dutta and M. A. Stroscio, Enhanced Signal-to-Noise in Photodetectors due to Interface Phonon-assisted Transitions, International Workshop on Computational Electronics, Paris, France, July 2014.

Yi Lan, Nanzhu Zhang, Lucy Shi, Chenjie Tang, Mitra Dutta and Michael A. Stroscio, Design of a Novel Heterostructure Photodetectors with Dramatically Enhance Signal-to-Noise based on Resonant Interface-Phonon-Assisted Transitions and Engineering of Energy States to Enhance Transition Rates, Optics-2014, 2nd International Conference and Exhibition on Lasers, Optics & Photonics, September 10, 2014 Philadelphia, USA (2014) (Invited)

Mitra Dutta, Ayan Kar, Mohsen Purahmad, Sidra Farid, Mojgan Mazouchi, Xenia Meshik, Michael A. Stroscio et al, Growth and characterization studies of oxide nanowires: Tin Oxide, Zinc Oxide and Indium Oxide, Optics-2014, 2nd International Conference and Exhibition on Lasers, Optics & Photonics, September 9, 2014 Philadelphia, USA (2014) (Invited)

M. Purahmad, M. A. Stroscio and M. Dutta, Modeling the Effect of Nanowire Size on the Piezoelectric Nanogenerators Output, International Workshop on Computational Electronics, Nara, Japan, June 2013.
N. Zhang, M. A. Stroscio and M. Dutta, Interface Phonon Modes of Dual-Gate MOSFET System, International Workshop on Computational Electronics, Nara, Japan, June 2013.
M. S. Choi, M. A. Stroscio, and M. Dutta, Effect of the Size and the Separation of Metal Nanodots on the Electromagnetic Enhancement to Surface-enhanced Raman Spectroscopy, International Workshop on Computational Electronics, Nara, Japan, June 2013.
Michael A. Stroscio, Mitra Dutta, Sicheng Liao, Banani Sen, Jun Qian, Robin Xu, Nanzhu Zhang, Min Choi, Yi Lan, Kimber Brenneman, Xenia Meshik, Preeti Pratap, and Donna Wu, Applications of Physics in Nanoscience and Nanoelectronics, Seminar at Ball State University, March 28, 2013.
Michael A. Stroscio and Mitra Dutta, Phonons in Nanostructures, University of New Mexico, May 2012.
Sushmita Biswas, Nanzhu Zhang, M. A. Stroscio, and M. Dutta, Conductive Polymer and Semiconducting Quantum Dots Nanocomposite Systems, International Workshop on Computational Electronics, Madison, Wisconsin, May 2012.
Banani Sen, M. A. Stroscio, and M. Dutta, Piezoelectric Fields in Quantum Wires, International Workshop on Computational Electronics, Madison, Wisconsin, May 2012.
M. Purahmad, S. Farid, M. A. Stroscio and M. Dutta, Influence of Piezoelectric Charges on the Surface Depletion Thickness of ZnO Nanowires, International Workshop on Computational Electronics, Madison, Wisconsin, May 2012.
M. Purahmad, S. Farid, M. A. Stroscio and M. Dutta, Influence of Substrates on the Optical Characteristics of ZnO Nanowires and Coreshell CdSe/ZnS Quantum Dots, International Workshop on Computational Electronics, Madison, Wisconsin, May 2012.
Sidra Farid, Michael A. Stroscio, Mitra Dutta, Raman Scattering Investigations of CdS Thin Films grown by Thermal Evaporation,PHONONS, 2012, July 8-12, 2012, Ann Arbor, Michigan.
Michael A. Stroscio, Mitra Dutta, Banani Sen, Ke Xu, Jun Qian, and Ke Sun, Phonons in Nanostructures, Phonon School, International Workshop on Computational Electronics, University of Wisconsin, June 2012; presentation included on the web report of the Phonon School at http://iwce2012.engr.wisc.edu/ (Invited)

Changes in research objectives (if any):

None

Change in AFOSR Program Manager, if any:

No recent changes; Dr. Kenneth Goretta is the Program Manager.

Extensions granted or milestones slipped, if any:

None

AFOSR LRIR Number

LRIR Title

Reporting Period

Laboratory Task Manager

Program Officer

Research Objectives

Technical Summary

Funding Summary by Cost Category (by FY, $K)

	Starting FY	FY+1	FY+2
Salary			
Equipment/Facilities			
Supplies			
Total			

Report Document

Report Document - Text Analysis

Report Document - Text Analysis

Appendix Documents

2. Thank You

E-mail user

Apr 26, 2015 22:31:21 Success: Email Sent to: stroscio@uic.edu